Natural variation reveals that intracellular distribution of ELF3 protein is associated with function in the circadian clock

M. Usman Anwer, Eleni Boikoglou, Eva Herrero, Marc Hallstein, Amanda M Davis, Geo Velikkakam James, Ferenc Nagy, Seth J Davis

DOI: http://dx.doi.org/10.7554/eLife.02206

Cite as: eLife 2014;10.7554/eLife.02206

Received: 3 January 2014
Accepted: 22 May 2014
Published: 27 May 2014

Natural variation reveals that intracellular distribution of ELF3 protein is associated with function in the circadian clock

Muhammad Usman Anwer[1,3], Eleni Boikoglou[1,2,a], Eva Herrero[1,b], Marc Hallstein[1], Amanda Melaragno Davis[1,3], Geo Velikkakam James[1], Ferenc Nagy[2] and Seth Jon Davis[1,3,c]

[1] Max Planck Institute for Plant Breeding Research, 50829, Cologne, Germany

[2] Biological Research Centre of the Hungarian Academy of Sciences, H–6726 Szeged, Hungary

[3] Department of Biology, University of York, York YO10 5DD, UK

[a] Present address: Cold Spring Harbor Laboratory, Laurel Hollow, NY 11791, USA

[b] Present address: MRC National Institute for Medical Research, NW7 1AA, London, United Kingdom

[c] Corresponding author: E-mail: davis@mpipz.mpg.de, seth.davis@york.ac.uk

Running title:

Circadian repression through ELF3 localization

Abstract:

Natural selection of variants within the *Arabidopsis thaliana* circadian clock can be attributed to adaptation to varying environments. To define a basis for such variation, we examined clock speed in a reporter-modified Bay-0 x Shakdara recombinant inbred line and localized heritable variation. Extensive variation led us to identify *EARLY FLOWERING3* (*ELF3*) as a major quantitative trait locus (QTL). The causal nucleotide polymorphism caused a short-period phenotype under light and severely dampened rhythm generation in darkness, and entrainment alterations resulted. We found that ELF3-Sha protein failed to properly localize to the nucleus, and its ability to accumulate in darkness was compromised. Evidence was provided that the *ELF3-Sha* allele originated in Central Asia. Collectively we showed that ELF3 protein plays a vital role in defining its light-repressor action in the circadian clock and that its functional abilities are largely dependent on its cellular localization.

Introduction:

The rotation of the earth leads to environmental changes in ambient light and temperature that define a 24-hour cycle. During these diurnal cycles, light is correlated with warmth, while darkness is correlated with coolness. Thus, to ensure fitness in response to such regular environmental oscillations, many organisms have evolved an internal timing mechanism to predict these cyclic environmental cues, and this is termed the circadian clock. This internal clock synchronizes major developmental and physiological processes. For example, a considerable proportion of metabolism is under clock control [1-4], and seasonal developmental programs require a circadian oscillator [5]. The coordination of molecular and physiological processes with the external environment thus provides an adaptive advantage under diverse climatic conditions [6].

Circadian rhythms are produced by molecular oscillators, which are comprised of interlocking feedback loops having several components [7]. In Arabidopsis, the central loop consists of two closely related single-myb transcription factors, CIRCADIAN CLOCK ASSOCIATED 1 (CCA1) and LATE ELONGATED HYPOCOTYL (LHY), as well as the pseudo response regulator (PRR) TIMING OF CAB EXPRESSION 1 (TOC1). In the morning, CCA1 and LHY repress *TOC1* by directly binding to its promoter, resulting in the evening accumulation of TOC1, which, in turn, represses *CCA1* and *LHY* expression [8,9]. The core oscillator is further tuned by an evening- and morning-phased loop. The evening loop is proposed to include GIGANTEA (GI) and TOC1, where GI activates the expression of *TOC1*, and TOC1 represses *GI* [9-11]. Two members of the pseudo response regulator gene family, *PRR7* and *PRR9*, repress *CCA1* and *LHY* during the day, and this establishes the morning loop [10,11]. Recently, an evening complex comprising EARLY FLOWERING 3 (ELF3), EARLY FLOWERING 4 (ELF4), and LUX ARRYTHMO (LUX) has been found to repress the morning loop by specifically binding to the *PRR9* promoter to mediate transcription repression [12-19].

Ambient light and temperature are two important environmental factors, termed *zeitgebers*, which reset the clock in a process referred to as entrainment [20,21]. PRR7 and PRR9 have been reported to play a role in temperature compensation, which is the resistance of period change under differing mean ambient temperatures [22,23]. However, diurnal temperature regulation of the circadian clock is still poorly understood [21]. In contrast, light has been established as a key factor for the entrainment of the clock where continuous irradiation shortens free-running period length in a fluence-rate-dependent manner as a process termed parametric entrainment [24-26]. Most genetic components of the clock were originally discovered from a light-entrained oscillator. Several studies have

shown that many observable rhythms in plants dampen in constant darkness (DD), where dampening is defined as a reduction in circadian amplitude. For example, many genes have been associated with circadian rhythms of mRNA abundance that are expressed robustly under constant light (LL), but dampen in DD [27,28]. Furthermore, the cyclic protein accumulation of several clock-regulated components, such as GI and ELF3 [29,30], was found to be reduced when shifted to darkness. Thus, the effects of various light-input signals on the Arabidopsis core oscillator remain to be elucidated.

Molecular and genetic studies support the involvement of ELF3 in light gating to the circadian clock, and ELF3 is also a required component of the core oscillator [16,25,31,32]. The *elf3* mutant was originally isolated in a screen for lines displaying photoperiod-independent early flowering [33,34]. Further characterization of *elf3* revealed other severe phenotypes, including defects in clock-regulated leaf movement rhythms, rhythmic hypocotyl elongation, and arrhythmic expression of gene expression under the free running condition of LL and in DD [16,31,32,35,36]. Natural variation at *ELF3* has been detected that could be associated to an alteration in shade-avoidance responses, which included increased elongation of the hypocotyl, delay of cotyledon opening in seedlings, increased elongation of stems and petioles, and reduced developmental timing in adults, and to changes in circadian function [47,48,49,62]. *ELF3* was cloned and reported to encode a nuclear protein of unknown function, and it was proposed to work as a transcription factor [30,37]. Based on the accumulation of ELF3 protein upon shifting plants to LL, and its decrease when plants were shifted to DD, it was concluded that its abundance is dependent on ambient light [30]. To extend this hypothesis based on the reported light-dependent phenotypes of *elf3*, McWatters *et al*. proposed that ELF3 fulfills the so-called *zeitnehmer* concept in that this factor acts to bridge light perception to the clock [38]. This idea was further strengthened when ELF3 was found to physically interact with the phytochromeB photoreceptor [30]. The previously noted role of ELF3 in light input to the circadian clock [31] is not altered by new findings that *ELF3* is core to the oscillator.

Many elements in the clock were isolated in screens for rhythm mutants using bioluminescence readout of the molecular oscillator. Worldwide, the species distribution of Arabidopsis ranges from the equator to extreme northern latitudes near the Arctic Circle [39]. Therefore, as an alternative to induced mutants, another source of genetic variation can be found among naturally occurring populations of Arabidopsis. More specifically, environmental variations across and within local populations of Arabidopsis act as a discriminatory force on the gene pool from which only a few genetic variants of adaptive phenotypes will be selected and pass through reproduction. Arabidopsis populations based on Recombinant Inbred Lines (RILs) have been derived from parental accessions. Such populations are advantageous in

mapping novel gene interactions. For example, quantitative trait locus (QTL) mapping was used to explain circadian parameters associated with natural variation in the circadian rhythmicity of leaf movement [40-43]. More recently, the rhythm of bioluminescence from modified firefly *LUCIFERASE* (*LUC*) genes coupled to the clock-controlled promoter was successfully used to map QTLs for circadian parameters [44,45]. Thus, the luciferase-based system can be employed to accurately measure variation in circadian-rhythm parameters within RIL populations to detect phenotypically expressed genetic variation in circadian clock genes [40].

In this study, we characterized a natural allele of *ELF3* to determine its effect on rhythmicity in the Arabidopsis circadian clock. Classical QTL mapping in a modified Bay-0 x Shakdara mapping population, followed by positional cloning, revealed an allele of *ELF3* (*ELF3-Sha*) that accelerates circadian oscillations in a light-dependent manner and a dampened oscillator in darkness, We determined that the periodicity phenotype of *ELF3-Sha* results from a single encoded amino-acid change A362V, which is an allelic variant that is largely confined to a latitudinal stripe in Central Asia. Furthermore, we identified that the circadian abnormalities in *ELF3-Sha* are associated to cellular localization defects of ELF3 protein that results in an inability to properly function under light and in darkness. Thus, by characterizing *ELF3-Sha*, we clarified the molecular mode-of-action of ELF3 in the circadian clock.

Results:

Analysis of circadian periodicity detected QTLs in Bay-0 X Sha RILS

A total of 71 RILs derived from the genetic cross of Bayreuth-0 and Shakdara (BxS) were modified to harbor the *CCR2* promoter, also termed *GRP7* [46], fused to luciferase (*CCR2::LUC*). These lines were synchronized to respective photic and thermal entrainment, and free-running periodicity was assessed under identical conditions of constant light and constant temperature. After applying both entrainment protocols, extensive variation in periodicity was observed (Figure 1A; Supplementary File 1; Supplementary File 2); however, the two parental ecotypes displayed similar periodicity, irrespective of preceding entrainment. Compared to photic entrainment, a significant shift for shortened free-running periodicity of *CCR2* after thermal entrainment was observed for the parental lines, as well as RILs (Figure 1A-C; Table 1). The periodicity differences after respective photic versus thermal entrainment [Period Light Dark (LD) - Period TMP (TMP)] extended from minus 0.56 hours to plus 1.66 hours (Figure 1B, C; Table 1), with parental lines displaying periodicity differences of plus 1.84 and plus 2.15 hours for Sha and Bay-0, respectively [44]. The averaged periodicity differences of BxS lines were moderate (0.433, $P<0.001$) (Table 1). Thus, despite the transgressive variation observed in the RILs for *CCR2* periodicity and periodicity differences (LD-TMP), the averaged periodicity differences seen in the RILs were similar in magnitude as the periodicity differences seen in the parental lines.

CCR2 free-running periodicity followed a normal distribution regardless of the entrainment *zeitgeber*, where lower and higher extreme periodicities were measured in thermal and photic entrainment, respectively (Figure 1A). The normally distributed phenotypes allowed us to test the fixed effects of entrainment (E) by the random effects of genotypes (G), and we found statistically significant G by E interactions (Table 2). The factor with the most significant effect in period variation was environment, with genotypes having a lesser, albeit highly significant effect (Table 2). Moreover, when the genotypic effect was compared between RILs and transformants, a far greater variation in periodicity could be observed in RILs (Table 2). Transformation-derived variation (position effects) was thus not a major component of detected variation. These findings suggest that both parents had been differentially selected in a number of loci for both *zeitgeber* inputs.

The significant effect of genotypes in periodicity prompted us to calculate trait heritabilities. These were found to be similar for photic (0.76) and thermal entrainment (0.73), respectively (Table 3). Our efforts then focused on mapping the genetic components of differential periodicity of the two inputs. This resulted in the identification of three large-effect QTLs for photic entrainment on chromosomes 1, 2, and 4. Two co-localized QTLs were

found on chromosomes 2 and 4 (Table 3). The QTL on Chromosome 2 (Chr2) displayed the largest phenotypic effect and we thus pursued its identification.

Fine-scale mapping identifies *ELF3* as a strong candidate for Chr2 QTL

To validate the identity of the Chr2 QTL, we generated heterogeneous-inbred families (HIFs), and near isogenic line (NIL). Three HIFs were made (57, 92 and 343; see Methods for construction details), each harboring either the Bay allele (HIF-Bay-0) or Sha allele (HIF-Sha) at the Chr2 locus. An analysis of the free-running period of these lines revealed that HIF-Sha always displayed a shorter period as compared to HIF-Bay-0. This period-shortening effect was independent of the preceding LD or TMP entrainment condition (Figure 2A). The complexities of the HIF genomic structure created the possibility for equally complex epistatic interactions that cannot be simply defined. Therefore, to circumvent the possibility of such interactions, a NIL with a small introgression of Sha at this Chr2 locus (NIL-S), in an otherwise homogeneous Bay genetic background, was generated. This line was measured for periodicity. Consistent with the HIFs, NIL-S displayed a 2h shorter period, as compared to Bay-0, which was only observed under LL. In DD, no significant period difference was detected (Figure 2B). However, in DD, the free-running profile of *CCR2::LUC* in NIL-S was different from the Bay parental line, so that, in NIL-S, *CCR2::LUC* rhythmicity lost robustness, whereas *CCR2::LUC* in Bay-0 displayed rhythms for seven days (Figure 3A). Interestingly, under both LL and in DD, the Sha parental line displayed a *CCR2::LUC* profile similar to that of Bay-0, and different from NIL-S (Figures 2B, 3A).

We next employed a fine-mapping strategy to isolate the Chr2 QTL and delineated the region to a 40Kb interval with nine annotated genes (Figure 2C). *ELF3* (AT2G25930) was the only gene in this region with a previously reported function in the Arabidopsis circadian clock. Therefore, we compared the sequence of *ELF3-Bay* and *ELF3-Sha* and identified two nonsynonymous changes in *ELF3-Sha*: an encoded alanine-to-valine transition at position 362 (A362V), and in the C-terminal encoded glutamine stretch, Sha had 8 more than Bay (Figure 3C; and as reported [47,48]). Thus, *ELF3* appeared as a strong candidate for the Chr2 QTL.

We then tested whether *ELF3-Sha* is involved in clock-controlled physiological processes under normal growth conditions. This was particularly relevant as it has been reported that the *ELF3* allele in Sha affects shade-avoidance responses [47-49]. To determine the sensitivity of *ELF3-Sha* to day length, as a basis of comparing to an *elf3* null allele, we examined the flowering time of the HIFs and NIL-S under long- and short-day

195 growth conditions, comparing the results to the Bay-0 wild type. While we observed no large
196 differences in flowering time under long days, HIF 89-S showed modestly advanced
197 flowering time under short days, compared to HIF 539-B (Figure 4A). Next we assessed the
198 effect of *ELF3-Sha* on hypocotyl length by measuring the hypocotyl length of HIFs, NIL-S,
199 Bay-0, Sha, and the null allele *elf3-1* under short days, constant red (RR), and constant blue
200 (BB) light. Similar to the near lack of flowering-time phenotype under long days, we did not
201 observe a substantial difference in the hypocotyl length of HIFs, NIL-S, and Bay-0 under RR
202 or BB. Under short days, however, HIF 89-S displayed a marginally elongated hypocotyl
203 length, compared to HIF 539-B, but this response was four times less than that seen in the
204 null *elf3* (Figure 4B). Overall, a NIL that harbored *ELF3-Sha* in a Bay background did not
205 display substantial physiological effects under normal growth conditions, indicating that
206 *ELF3-Sha* maintains developmental activity lost in null *elf3* alleles.

207

208 **Alanine to Valine substitution underlies *ELF3-Sha* circadian phenotypes**

209 Although fine-scale mapping provided strong evidence favoring *ELF3* as the gene
210 responsible for the short-period phenotype we observed, any one of the nine genes in the
211 40kb region were candidates in the context of this study. Therefore, to generate genetic
212 materials to test if *ELF3-Sha* was indeed the causal QTL, we cloned *ELF3*, along with its own
213 promoter from Bay-0 and Sha, fused these with *YFP*. These constructs were then
214 transformed to the null allele *elf3-4* in the Ws-2 background, harboring *CCR2::LUC* and
215 *LHY::LUC* reporter genes, respectively. The free-running period analysis of T2 transgenic
216 lines harboring *ELF3-Sha-YFP* displayed a consistent short period under LL, compared to
217 the lines harboring *ELF3-Bay-YFP,* for both *LHY::LUC* and *CCR2::LUC* (Figure 3B). Based
218 on these complementation experiments, we confirmed *ELF3* as quantitative trait gene (QTG)
219 underlying the Chr2 periodicity QTL.

220 To define the causal polymorphism in *ELF3-Sha*, we investigated the role of an
221 encoded A362V residue change compared to the difference in the number of encoded
222 glutamines in *ELF3-Bay* and *ELF3-Sha*. In this experiment, we separately cloned the
223 promoter and coding regions of *ELF3-Bay* (SpBc) and *ELF3-Sha* (SpSc) and then induced
224 encoded A362V and V362A changes in *ELF3-Bay* (SpBa2v) and *ELF3-Sha* (SpSv2a) coding
225 regions, respectively. These constructs were then recombined in all possible
226 promoter::coding combinations (illustrated in Figure 5A). The free-running period of
227 *LHY::LUC* in T2 transgenic lines harboring different coding regions, under the control of the
228 *ELF3* promoter of the Sha accession, was analyzed under LL. We observed that lines SpSc
229 and SpBa2v that contained encoded valine displayed a shorter period as compared to the

SpBc and SpSv2a lines harboring encoded alanine, irrespective of the number of glutamines present (Figure 5B). We further confirmed these results in the transgenic lines expressing *ELF3-Bay* and *ELF3-A362V* under the Bay-0 *ELF3* promoter. The free-running profile of *LHY::LUC* was analyzed under LL and in DD. Both *ELF3-Bay* and *ELF3-A362V* displayed a robust rhythm of *LHY::LUC* expression under LL, albeit with lower amplitude observed in *ELF3-A362V* (Figure 5C). However, in DD, the expression profile of *LHY::LUC* in *ELF3-Bay* and *ELF3-A362V* was distinctly different. *ELF3-A362V* failed to maintain robust rhythms after four days in darkness and displayed an acute dampening of *LHY::LUC* expression, whereas *ELF3-Bay* displayed robust rhythm of *LHY::LUC*, even after 6 days in darkness (Figure 5D). The period analysis of *LHY::LUC* expression in *ELF3-Bay* and *ELF3-A362V* revealed no statistically significant period difference in DD, whereas under LL, *ELF3-A362V* displayed a shorter period compared to *ELF3-Bay* (Figure 5E). These results are consistent with those described above for both HIFs and NIL-S and support that the encoded A362V polymorphism is the functionally encoded variant in Sha sufficient to explain the Chr2 periodicity QTL in the BxS population (Figure 2A, B). Thus, we could explain the molecular basis of a clock periodicity QTL to an absolute level of a single nucleotide, colloquially defined as the "quantitative trait nucleotide" (QTN).

Alanine362 is a required residue to sustain robust rhythmicity in darkness

To further dissect the effect of light and darkness on *ELF3-Sha*, we measured *LHY::LUC* expression in *ELF3-Bay* and *ELF3-A362V* for fifteen days with a defined regime of extended light and darkness. We observed that both *ELF3-Bay* and *ELF3-A362V* displayed robust *LHY::LUC* expression so long as they remained under light (Figure 6A). However, when the plants were transferred to darkness, *LHY::LUC* expression dampened more rapidly in *ELF3-A362V*. For *ELF3-Bay*, an acute reduction of *LHY::LUC* expression was seen such that proper rhythm was maintained throughout the dark period, while no detectable rhythmic expression of *LHY::LUC* was observed in *ELF3-A362V* (Figure 6A). To test if the loss of rhythm of *LHY::LUC* in *ELF3-A362V* was light-dependent or resulted from a "permanent" defect in the clock caused by continuous darkness, we subsequently returned these plants to light after an interval of 4 days in darkness. Both *ELF3-Bay* and *ELF3-A362V* recovered robust rhythms of *LHY::LUC* after the 11-day treatment, including the 4-day period in darkness (Figure 6A). These results suggested that light is necessary to sustain a robust oscillator in the context of *ELF3-A362V*.

Rhythmic robustness depends on the precision of the circadian clock, and relative amplitude error (R.A.E.) is a measure of such precision [17]. Therefore, to test the precision

of *LHY::LUC* expression rhythms in *ELF3-Bay* and *ELF3-A362V*, we estimated the period and R.A.E. of these lines under LL and in DD. Under LL, *ELF3-A362V* displayed a ~1.5h short period compared to *ELF3-Bay*, with both lines showing high precision (R.A.E. < 0.20; Figure 6B and 7A, ZT40-120). However, in darkness, while both lines had similar period estimates, *ELF3-A362V* did not maintain precision and displayed high R.A.E. (R.A.E. > 0.75), compared to *ELF3-Bay* (R.A.E. < 0.35; Figures 6B and 7B, ZT160-240). Interestingly, the loss of precision of *LHY::LUC* rhythm was recovered in *ELF3-A362V* when the plants were returned to the light at ZT250 (Figures 6B and 7C, ZT260-340). This restoration of precision led us to hypothesize that in darkness the clock remains partially functional in *ELF3-Sha* in the context of this low precision. To confirm this, we performed an experiment where the phase of *ELF3-Bay* and *ELF3-A362V* lines was estimated after resumption of plants to LL that were previously subjected to different intervals of darkness. We reasoned that if the *ELF3-A362V* plants are truly arrhythmic in DD, then the circadian phase after resumption of light should be determined solely by the exposure to light and not by the duration of the dark period. For *ELF3-Bay*, with a more functional clock in the dark, the phase will be determined in part by the duration of dark exposure. We found that *LHY::LUC* peaked at a similar time in both *ELF3-Bay* and *ELF3-A363V*, which in part was determined by the duration of the dark period. This revealed the presence of a partially functional oscillator during the dark period in both these lines. Further, no significant phase difference between these lines was detected at any time point tested (Figure 8A). Interestingly, consistent with the above results (Figure 5A), once the plants were transferred back to the light, robust rhythms of *LHY::LUC* were restored (Figure 8B). Notably, in a phase-difference graph (Phase *ELF3-Bay* minus Phase *ELF3-A362V*), a consistent pattern of phase oscillations was detected, supporting the existence of a functional oscillator in both *ELF3-Bay* and *ELF3-A362V* that display differences in their respective resetting behavior (Figure 6C). This confirms that ELF3-Sha contributes to light-input to the clock, but displays differences in its "*zeitnehmer*" entrainment capacity. Taken together, we concluded that *ELF3-Sha* requires light input to maintain precision of the circadian clock; however, darkness does not fully abolish the low-amplitude oscillation in *ELF3-Sha* plants and that entrainment processes appear altered.

ELF3-Sha **is defective in proper clock resetting**

In Arabidopsis, light input to the circadian clock follows Aschoff's rule who noted that the activity phase shortens in nocturnal organisms exposed to constant light conditions and lengthens in diurnal organisms [24]. These trends were termed alpha compression and alpha expansion, respectively. This process is also known as parametric entrainment [24,26].

ELF3, as a repressor of light signaling to the clock, is expected to be involved in such parametric entrainment [25]. In the past, the availability of null mutants precluded testing such a hypothesis. However, the fact that *ELF3-Sha* is a functional allele could be advantageous in determining if *ELF3* is involved in parametric entrainment. To test this, we measured the free-running period of Bay and NIL-S under an array of fluences, including RR, BB, and "white" (RB) light. Under diverse intensities and qualities of light, we found that NIL-S displayed a shorter period than Bay. Moreover, both Bay and NIL-S followed Aschoff's rule, displaying shortening of periodicity with increase in fluence rate (Figure 9A-C). From these results, one of two conclusions may be drawn: 1) that ELF3 is not directly involved in parametric entrainment or 2) that the *ELF3-Sha* allele is fully functional in discriminating between different light intensities.

An important characteristic of clock entrainment is termed frequency demultiplication, which describes the resetting properties of the oscillator. Wild-type plants with a functional clock entrained under 24h environmental cycles (T24) maintain the same rhythms when transferred to shorter cycles (T12). In this way, plants resist the resetting of the oscillator by sporadic environmental changes during a diurnal cycle. However, if the short cycles (T12) persist, a robust clock should reset to the new environment. Conversely, when transferred from T24 to T12, mutants with a dysfunctional clock promptly follow the shorter cycles [18,31,32]. To test the demultiplication ability of *ELF3-Sha*, we monitored *LHY::LUC* expression for 7 days in *ELF3-Bay*, *ELF3-A362V*, Ws-2, and *elf3-4* lines under T12 cycles (6h light and 6h dark) after initially entraining under T24 cycles (12h light and 12h dark). As previously reported for null *elf3* [31], we detected a driven 24h rhythm, and, thereafter, *LHY::LUC* completely followed the T12 cycles in this mutant, revealing, in turn, a dysfunctional clock (Figure 6D). As expected, both Ws-2 and *ELF3-Bay* initially resisted the T12 cycles for 3 days, displaying driven T24 rhythms. However, after 3 days, both Ws-2 and *ELF3-Bay* showed a robust adaptation to the T12 cycles, which were observed as strong *LHY::LUC* peaks matching the peaks expected for T12 cycles (Figure 6D). Interestingly, *ELF3-A362V* did not show this effect in T12 cycles, and strong *LHY::LUC* peaks completely matched the T24 cycles for all 5 days (Figure 6D). Since both Ws-2 and *ELF3-Bay* responded to persistent T12 cycles, while *ELF3-Sha* did not, we concluded from these results that *ELF3-Sha* failed to perceive persistent new environmental signals, revealing that the circadian oscillator in *ELF3-Sha* is indeed defective in proper entrainment resetting.

Compromised clock network in *ELF3-Sha*

Under continuous light and in darkness, it has been reported that *elf3* loss-of-function alleles display arrhythmia [32,35]. Accordingly, expression profiling revealed that *elf3* had reduced expression of the core oscillator genes *CCA1* and *LHY*, but high levels of the evening genes *TOC1* and *GI* [13,50,51]. As these null *elf3* studies were conducted in the context of arrhythmia, placing *ELF3* in the clock network has been difficult. However, as *ELF3-Sha* displayed rhythmicity (Figure 5C), we monitored the luciferase reporter expression profile of the central clock genes *CCA1*, *LHY*, *TOC1*, *GI, PRR7,* and *PRR9* in NIL-S and compared it with Bay-0 wild type and the null mutants *elf3-1* and *elf3-4* under both LL and DD. Consistent with previous reports [13,16,31,32,51], both null mutants, *elf3-1* and *elf3-4*, displayed arrhythmia with reduced levels of *CCA1::LUC* and *LHY::LUC* and high levels of *TOC1::LUC*, *GI::LUC*, *PRR7::LUC,* and *PRR9::LUC,* compared to Bay-0 (Figure 10). Consistent with the short-period phenotype of *CCR2::LUC* in NIL-S (Figure 2B), all clock genes also displayed a short-period phenotype (Figure 10 A-F). The comparison of expression profiles of these clock genes in NIL-S, *elf3-1*, *elf3-4* and Bay-0 revealed an intermediate effect of *ELF3-Sha*. Specifically, in NIL-S, the expression of *CCA1::LUC* and *LHY::LUC* was higher than that of *elf3-1* and *elf3-4,* but lower than that of Bay-0. Similarly, the expression of *TOC1::LUC*, *GI::LUC, PRR7::LUC,* and *PRR9::LUC* in NIL-S was lower than that of *elf3-1* and *elf3-4*, but higher than that of Bay-0 (Figure 10 A-F). Similar to LL, profiles of luciferase expression for clock genes with reduced levels in DD were observed in NIL-S, *elf3-1*, *elf3-4* and Bay-0, except that of *TOC1::LUC* in NIL-S, which was high and comparable to the null mutants (Figure 10 G-L). A continuous increase in the expression of *GI::LUC* in NIL-S was also observed. No significant period difference was observed in NIL-S and Bay-0 in any clock gene under DD. Consistent results were also obtained when we confirmed the luciferase expression data by monitoring the transcript profile of these genes under LL (Figure 11). Unlike *elf3-1* and *elf3-4* loss-of-function mutants, our cumulative results indicate that *ELF3-Sha* is a hypomorphic allele capable of sustaining the oscillation network.

Cellular basis of *ELF3-Sha* short-period phenotype

A higher expression of morning genes, *PRR7* and *PRR9*, and evening genes, *TOC1* and *GI*, suggests a repressive role of *ELF3*. Thus, the short-period phenotype of *ELF3-Sha* could be caused by a reduced level of *ELF3* transcript or protein accumulation. To test this, we first measured the transcript accumulation of *ELF3* and then assessed the amount of protein generated. We found that the mean level of *ELF3-Sha* transcript was slightly higher relative to *ELF3-Bay* (Figure 13C). Correspondingly, higher ELF3-Sha protein accumulation

was detected in comparison to *ELF3-Bay*, as measured by the ELF3-YFP signals (Figure 12 A-D). As increases in ELF3 drives a long period [16,25], elevated protein levels in *ELF3-Sha* thus did not explain the short-period phenotype. Importantly, a more detailed comparison of ELF3-Bay-YFP and ELF3-Sha-YFP revealed differences in cellular localization. Specifically, the formation of distinct nuclear bodies, a characteristic of ELF3 [16], was markedly attenuated in ELF3-Sha, whereas these nuclear bodies were clearly observable in ELF3-Bay (Figure 12 A,B). Additionally, the preferential nuclear localization of ELF3 was compromised in ELF3-Sha, which displayed a markedly elevated amount of cytoplasmic content, compared to ELF3-Bay (Figure 12 A-D). Quantification of YFP revealed that the nuclear-cytoplasmic ratio of ELF3-Sha was four times less than that of ELF3-Bay (Figure 12E). As such, we proposed that these localization defects of ELF3-Sha underlie its oscillator defects.

Having shown that ELF3-Sha is defective in proper cellular localization, we next sought to identify if the localization aberrations cause faulty regulation of ELF3-Sha. This is particularly relevant as it has been shown that ELF3 accumulates under light, but quickly dissipates in darkness by proteasomal machinery involving the action of COP1 and GI. Furthermore, both these proteins physically interact with ELF3 to form similar nuclear bodies that are presumed to be their point of interaction [52]. As such, it could be anticipated that the lack of formation of such nuclear bodies in ELF3-Sha might result in its dysregulation. To examine such a possibility, we monitored the patterns of *ELF3* transcript and protein accumulation over a diurnal cycle under LD compared to the same patterns under LL and in DD. Under LD, we found only a minor increase in *ELF3-Sha* transcript and protein levels compared to *ELF3-Bay* (Figure 13 A,B). However, under LL, the *ELF3-Sha* transcript was significantly higher at all time-points compared to *ELF3-Bay,* which also resulted in elevated levels of ELF3-Sha protein (Figure 13 C,D). Furthermore, compared to LD where ELF3 accumulation decreased during the evening hours, we found elevated protein levels of both ELF3-Bay and ELF3-Sha during subjective night (ZT16 and ZT20). These results were consistent with previous reports that ELF3 accumulation increases in light [30,52]. In DD, similar to LL, *ELF3-Sha* transcript levels were higher compared to *ELF3-Bay*. However, we did not detect any significant difference in ELF3-Bay and ELF3-Sha protein levels during subjective day, whereas during subjective night (ZT16 and ZT 20), we found that ELF3-Sha accumulation was considerably lower than ELF3-Bay (Figure 13 E, F). Taken together, a higher accumulation of ELF3-Sha under LL and overall lower levels in DD, despite higher transcript abundance, led us to conclude that ELF3-Sha protein dissipates in darkness comparatively more rapidly than ELF3-Bay.

Allelic diversity at the *ELF3* locus

Finally we sought to identify the evolutionary history of the *ELF3-Sha* locus. To accomplish this, we retrieved the *ELF3* coding sequence (CDS) of 251 accessions from the "1001 Genome- Project" (see methods) and performed several population-genetics analyses. The sequence comparison revealed the presence of 59 polymorphic sites segregating at the *ELF3* locus, including encoded A362V. Out of these 59 polymorphic sites, 16 were synonymous and 43 were nonsynonymous. The A362V was detected in 15 accessions, and in a phylogenetic analysis, all of these grouped together in a single clade, suggesting a common origin (Figure 14A). Therefore, we looked at the geographical distribution of these accessions and found that they all were distributed in Central Asia between 37°N to 54°N, with two exceptions at Nemrut and Rubenzhoe collected from Turkey and the Ukraine, respectively (Figure 14B, Table 4). Interestingly, similar to Sha that naturally grows at high altitudes (*e.g.*, Pamir Mountains, Tajikistan), most of these accessions were also high-altitude accessions collected in the mountains (Table 4). These results suggest that *ELF3-Sha* originated from Central Asia and that this allele might has been maintained during species migration preferentially by altitude-associated individuals.

Discussion:

ELF3 has been established as a required component for the generation of circadian rhythms and the perception of light and temperature inputs [25,31,32]. However, most of the *elf3* alleles used in these studies were identified in mutagenesis screens, and many of them displayed arrhythmicity under free-running conditions of LL and DD. Here, we report the cloning and characterization of *ELF3-Sha* as a natural allele of *ELF3*, which displayed a light-dependent short-period phenotype. Unlike *elf3* loss-of-function mutants, this allelic state displayed robust circadian rhythms under continuous light. However, in prolonged darkness, the expression profile of many clock genes was dramatically damped (Figure 10). The association between the clock phenotypes of *ELF3-Sha* and their cellular basis led us to conclude that proper cellular distribution of ELF3 is required to perform normal repressive function in the circadian clock (Figures 12, 13) which in turn, depends on its cyclic accumulation. Importantly, we could track the origin of *ELF3-Sha* to Central Asia, providing more insight about the molecular evolution of this allele.

The identification and validation of quantitative trait loci (QTLs) by genetic mapping is a well-established procedure. However, to understand the molecular basis of a locus by characterizing QTL to a quantitative trait nucleotide (QTN) level is still an arduous task [39]. Here we reported the characterization of a natural allele of *ELF3 (ELF3-Sha)* to a QTN level of understanding. In the quantitative analysis of circadian periodicity of a modified BxS population, we identified a QTL and further validated it in HIFs and a NIL (Table 1, Figure 2A, B). Our periodicity results were consistent with previous studies where the *ELF3* in Sha was found to modulate the shade-avoidance response, including the action of shade on the oscillator [47,49]. In those studies, HIFs were the main genetic resource used. The authors of those papers proposed *ELF3* to be a candidate locus for the detected shade-avoidance QTL, and transgenic efforts were used to complement that notion [49]. Here we generated the appropriate NIL and showed that the introgression of *ELF3-Sha* to Bay-0 resulted in severe circadian alterations, including a curtailed period length (Figure 2B, A).

The light-dependent acceleration of circadian oscillations of *ELF3-Sha* could be associated with reduced ELF3 functionality [25,31,38]. The intermediate expression profile of several clock genes in *ELF3-Sha,* when compared to wild type and null mutants, confirmed that it is a hypomorphic allele (Figures 10, 11). This characteristic of *ELF3-Sha* is distinctly different from *elf3* null mutants, which displayed complete arrhythmia under LL [25,31,32,37]. However, the functionality of the oscillator in these mutants in darkness remained disputable. Based on the observation that the circadian rhythms persist in the *elf3-1* mutant, it was proposed that ELF3 solely acts as a light *zeitnehmer*, or timekeeper, and that it is not a

456 required component of the oscillator. In contrast, a recent study reported that the circadian
457 oscillator was abolished in constant darkness (DD) in temperature-entrained *elf3-1* seedlings,
458 emphasizing that ELF3 is an integral part of the oscillator as well as acting as a *zeitnehmer*
459 [32]. As these studies were mainly based on null mutants, a conclusive statement about
460 ELF3 function in sustaining the oscillator in DD is hard to draw. Consequently, in this paper,
461 we thus analyzed the profile of several clock genes in the functionally stable *ELF3-Sha*
462 mutant in DD, comparing it with those in *elf3-1* and *elf3-4* null mutants. Consistent with a
463 previous report [32], we could not detect any sign of rhythmicity in null *elf3* mutants.
464 Interestingly in the hypomorphic *ELF3-Sha*, a rapid dampening in the expression of several
465 clock markers in DD was observed (Figures 3A, 5D, 6A, and right panels of Figure 10G-L).
466 Thus, our results conclusively demonstrate that ELF3 is required for robust oscillation in
467 darkness and further support the idea that ELF3 is an integral part of the oscillator [32].
468 Although *ELF3-Sha* lost robustness and precision in prolonged darkness, it is important to
469 note that it quickly recovered when transferred back to the light (Figures 6A, 6B, 7A-C).
470 Consequently, we further propose that the function of *ELF3* is collectively defined by both the
471 light-dark boundary and by circadian clock regulation.

472 *elf3* loss-of-function mutants under free-running conditions were previously shown to
473 display major defects in the expression of the core oscillator genes *PRR7*, *PRR9*, *CCA1*,
474 *LHY*, *TOC*1, and *GI* [13,31,51]. To monitor the expression of these clock genes in *ELF3-Sha*,
475 we used the robust luciferase reporter-expression system and measured these expression
476 profiles in Bay-0, NIL-S, and the nulls *elf3-1* and *elf3-4*. Our results were consistent with
477 previous reports showing the arrhythmic low levels of *CCA1* and *LHY* and high levels of
478 *TOC1* and *GI* in *elf3* loss-of-function mutants. In contrast, under LL, *ELF3-Sha* was rhythmic
479 for all genes studied, and it displayed an intermediate level of expression compared to wild
480 type and loss-of-function *elf3* (Figure 10 A-F, left panels). Specifically, NIL-S displayed higher
481 expression of *TOC1* and *GI* compared to Bay-0, but lower expression than *elf3-1* and *elf3-4*.
482 In contrast, expression of *CCA1* and *LHY* was lower in NIL-S, compared to Bay-0, but higher
483 than *elf3-4*. Consistent with the previous finding that CCA1 and LHY regulate *PRR7* and
484 *PRR9* [53,54], a higher transcript abundance of *PRR7* and *PRR9* was observed in NIL-S
485 (Figures 10 E,F and 11C,D). These data, along with recent findings showing the evening
486 complex (*ELF3*, *ELF4*, and *LUX*) directly binds to the *PRR9* promoter to repress
487 transcription, support the repressive action of ELF3 in the core oscillator [12,14,16,19].
488 Higher expression levels of the evening genes *TOC1* and *GI*, as well as dramatically
489 dampened oscillations of *ELF3-Sha* in darkness, cannot be simply explained by only
490 considering ELF3 at *PRR9*. Considering the double loss-of-function mutant *cca1-11 lhy-21* is
491 rhythmic, an additional repressive role of ELF3 by targeted degradation of GI is conceptually

plausible [52,55]. Taken together, our data support a hypothesis which holds that the EC-containing ELF3 has more than one entry point in the circadian clock [15,17,31].

ELF3 is both a cytosolic and nuclear localized protein. It appears to be multifunctional in that it has several binding partners. These include phyB, COP1, ELF4, and GI [16,19,52]. Different domains of ELF3 specifically interact with these different proteins. Both phyB and COP1 interact with the N-terminal domain [30,31,52], whereas ELF4 and GI interact with the middle domain [16,52]. Further, all these proteins co-localize in the nucleus where they form distinct nuclear bodies [16,52,56,57]. Such nuclear foci could be suspected as interaction points of binding proteins [15,16,52,58]. Thus, formation of fewer ELF3-nuclear foci from encoded *ELF3-Sha* might be the result of a defect in the binding of one of its interacting proteins. Since the A362V variant is located in the middle domain of ELF3, such a hypothesis could be particularly attributed to either GI and/or ELF4. The rhythmic accumulation of both ELF3 and GI depends upon the activity of COP1 that mediates ubiquitination and targeted degradation of these proteins in dark conditions [52]. It is noteworthy here that ELF3 is essential for this process. In absence of ELF3, COP1 cannot interact with GI and thus cannot initiate its decay. However, GI is not required for COP1-mediated ELF3 degradation [52]. When these data are taken together, the formation of a COP1-ELF3-GI complex could be considered a plausible active mechanism controlling the rhythmic accumulation of these proteins. Under these conditions, A362V mutation in *ELF3-Sha* would result in attenuated binding affinity with GI, disturbing the balance of the COP1-ELF3-GI complex and, in turn, resulting in the rapid decay of ELF3. Both the lower accumulation of ELF3-Sha protein, despite the generation of higher transcript (Figure 13E, F), and aberrant oscillator behavior of ELF3-Sha in prolonged darkness support this hypothesis. The short-period phenotype of *ELF3-Sha* under LL could also be explained by an early decay of ELF3-Sha during light/dark entrainment. As ELF3 directly represses *PRR9* [13,16], the early depletion of ELF3-Sha results in an early expression of *PRR9*, an event that sets the pace of the oscillator during the preceding entrainment, which is maintained through LL. Based on these results and our observation that *ELF3-Sha* is defective in proper clock resetting (Figure 6D), we propose that ELF3 plays a pivotal role in defining entrainment properties of the circadian clock, which, in turn, depend on cyclic accumulation of ELF3 protein, but not on its absolute levels or, indirectly, its transcript abundance. This idea could be further supported by the observation that ELF3 protein rhythmically oscillates and drives a long period in plants that constitutively overexpress *ELF3* [13,16,25]. Discounting the important role that ELF3 plays in clock entrainment, it can be provisionally excluded that ELF3 is involved in parametric entrainment because we could not detect any differential effect of fluence rate on *ELF3-Sha* periodicity

compared to *ELF3-Bay* (Figure 9A-C). Fluence rate curves based on *ELF3-ox* also support this notion [25].

Studies on *ELF3-Sha* as a natural allele disrupted in normal circadian behavior provide a perspective on its repressive action on clock periodicity. Notably, in the context of the Ws-2 and Bay-0 genomes, we could show that *ELF3-Sha* is a hypomorphic allele defective in proper localization of encoded ELF3 protein. This defect resulted in two distinct phenotypes: one displaying a light-dependent short period and the other exhibiting loss of rhythm robustness in darkness. These phenotypes were clearly observable in both the Bay-0 and Ws-2 genetic background. It is notable that Sha parental line did not itself display such obvious circadian defects (Figure 2B, 3A). Related to this, the transcript profile of clock genes in Sha followed the same pattern as observed in Bay-0, and such pattern was distinct from that seen in NIL-S (Figure 11). Moreover, *ELF3-Sha* did not affect hypocotyl length in NIL-S and Sha in the same way. Under all light qualities tested, the hypocotyl length of NIL-S was similar to that of Bay-0, but was significantly longer when compared to Sha (Figure 4B), leading to the possibility that other segregating QTLs within Sha wild type genetically interact with *ELF3-Sha*. Such similar background-dependent effects of natural alleles have been reported in Arabidopsis for seed longevity, axillary bud formation, and flowering time [59-62].

Our efforts to track the history of the *ELF3-Sha* revealed that this allele is present in a group of genetically related accessions that are predominately distributed in a geographical area of Central Asia (Figure 14A, B). This confined location of *ELF3-Sha* leads to the possibility that this allele provides local adaptive advantage to these accessions under their respective environmental conditions, and thus, has been positively selected during species migration. Such a hypothesis can only be confirmed in further studies using realistic environmental conditions in which these accessions are derived.

Materials and methods:

Plant material

The Recombinant Inbred Lines (RILs) used were derived from the Bayreuth-0 (Bay-0) by Shakdara (Sha) RIL collection (termed here BxS) [46]. Multiple, independent T1 transgenic *CCR2::LUC* reporter lines were obtained from 69 lines after floral dipping [44,74]. T2 progeny were used for circadian rhythm experiments (Supplementary files 1 and 2). To confirm the chromosome 2 periodicity QTL in BxS, three heterogeneous inbred families (HIFs) were generated. For this, RILs 57, 92, and 343 were used as recipients of a pollen donation from Bay-0 *CCR2::LUC*. These F1 lines were respectively backcrossed twice to the given RIL. In these three BC2 populations from the separate RIL crosses, the plants were self-crossed, and in the derived BC2F2 populations, lines that were homozygous for Bay or for the Sha alleles, at four marker positions, were identified. Multiple F2 versions of each of these derived lines were isolated. F3 seeds that harbored *CCR2::LUC* were collected from these plants for periodicity tests, as described below. The selected F3 HIFs containing Sha at QTL interval were further backcrossed three times to Bay-0 to generate NIL-S. The introgression of Sha at QTL interval and the homogeneous Bay-0 background were confirmed with genome-wide SSLP markers. For fine mapping, the progeny of HIF343, heterozygous at QTL interval, was screened with different SSLP, CAPS, and dCAPS markers. Out of 1100 plants screened, 14 plants with a recombination event between markers elf100L and elf100R were selected and self-fertilized to obtain homozygous recombinant lines. The progeny of these homozygous recombinant lines was then used for circadian-periodicity assay. The detail of all the markers used for genotyping is given in Table S3.

The mutant lines used in this study were as follows: *elf3-1* and *elf3-4* [33,34,37]. Both mutant lines were backcrossed four times to the Bay-0 wild type to homogenize the accession background to Bay-0. Homozygous plants were subsequently identified in the BC4F2 population using specific markers (Table S3). Different clock-marker lines, *CCR2::LUC*, *CCA1::LUC*, *LHY::LUC*, *TOC1::LUC*, and *GI::LUC*, used in the study were generated by initial transformation of the respective marker into Bay-0, followed by crossing the T2 transformants to the target genotype: Bay-0, NIL-S, *elf3-1*, and *elf3-4*. The homozygous lines obtained by the self-fertilization of BC1F2 were used for the circadian assays.

To generate *ELF3 Bay* transgenic lines, the *ELF3* gene, along with *ELF3* native promoter, was amplified from Bay-0 genomic DNA and cloned into pPZP211 vector. In *ELF3 A362V*, a nucleotide change encoding Alanine to Valine (A362V) was induced using the

QuikChange method (Stratagene). The multi-gateway technology (Invitrogen) was used to generate the YFP-tagged lines with different promoter-coding combinations. Initially, the promoter and coding regions of *ELF3* were separately amplified from Bay-0 and Sha genomic DNA and recombined into pDONR4-P1R or pDONR201 donor vectors, respectively. The respective nucleotide change encoding either the A362V or V362A amino acid was then induced using the QuikChange method (Stratagene). The YFP tag was separately cloned into pDONRp2r-p3 donor vector. These three donor vectors were then recombined in different combinations into pPZP211 destination vector. The final vector was then transformed into *Agrobacterium tumerfaciens* (strain ABI). For all transformations, the improved floral-dip method was used [63]. Based on Mendelian segregation, T2 transgenic lines having single insertion were selected on kanamycin. All the transgenic lines harboring *ELF3-Bay, ELF3-A362V, ELF3-Bay-YFP, ELF3-Sha-YFP, SpSc, SpBc, SpBa2v* and *SpSv2a* are in *elf3-4 Ws-2* genetic background. All oligonucleotides used for cloning and QuikChange are listed in Supplementary File 3.

Plant growth conditions, luciferase assay, and measurement of developmental traits:

For LUC assays, seeds were surface-sterilized and plated on MS medium containing 3% sucrose. Following ~3 days stratification at 4°C, seedlings were entrained for 7 days, either under 12L:12D cycles (~100μE light) with constant temperature of 22°C (LD) or under 12h at 16°C: 12h of 22°C temperature cycles with constant light (TMP) (~100μE light). The bioluminescence measurement and data analysis are as described [64,65]. For hypocotyl assays, seedlings were grown on MS medium (2.2g/L pH 5.7) without sucrose, as described [66]. Hypocotyl length was determined for seedlings grown under SD (8L:16D), BB, or RR for 7 days (light intensity SD: 120 μmol m-2s-1; light intensity RR and BB: 15 μmol m-2s-1). Seedlings were scanned, and hypocotyl elongation was measured using the ImageJ 64 program, V1.43b (Wayne Rasband, National Institutes of Health, USA, http://rsb.info.nih.gov/ij). For flowering time measurement, plants were grown on soil containing a 3:1 mixture of substrate and vermiculite in a temperature-controlled greenhouse environment with 16L:8D long-day and 8L:16D short-day cycle. The flowering time was scored at the time of bolting (1cm above rosette leaves) as the total number of days to bolt [67].

QTL mapping and analysis:

In total, 60 and 65 BxS lines were assayed for *CCR2* rhythmic periodicity after light and temperature entrainment, respectively. Period mean was subsequently used for QTL mapping, which was performed with MapQTL 5.0 (Kyazma B.V., Wageningen, The Netherlands). Mapping settings used were as in [44]. The statistical analyses, including broad sense heritability were calculated as reported [44,68].

Confocal microscopy:

For all microscopic work, the Zeiss LSM700 confocal microscope from Carl Zeiss was used, as in [16]. Briefly, the plants were grown on MS medium containing 1.5% sucrose. Following ~3 days stratification at 4°C, seedlings were entrained for 6 days under 12L:12D cycles (~100μE light) with constant temperature of 22°C. The following day, the plants were either put under constant light (LL: ~100μE light) or in darkness for another day. On day 7, starting at ZT0, the plants were scanned, and the photographs were taken every 4 hours for one day. For the comparison of *ELF3 Bay-YFP* and *ELF3 Sha-YFP* lines, one slide from each line was prepared, and both slides were put together in the microscope. The plants from each slide were then scanned, one after another, within 30 minutes and with the same microscope settings. The microscope settings for the Figure 13 dataset were as follows: Image size: x = 512, y = 512, z = 20; Channels: 3, 8-bit, Zoom = 1.0; Objective: Plan-Aprochromat 40x/1.30 Oil; Pixel dwell: 2.55μs; Master gain: ch1= 972, ch2= 847, ch3= 162; Digital gain: ch1 = 1.20, ch2 = 1.0, ch3 = 1.50; Digital offset = ch1 = -18.0, ch2 = 2.0, ch3 = -24.42; Pinhole = 156μm; and laser: 488nm with 10.0% strength. For the Figure 12 dataset, microscope settings were as follows: Image size: x = 512, y = 512, z = 20; Channels: 3, 8-bit, Zoom = 0.5; Objective: Plan-Aprochromat 63x/1.40 Oil; Pixel dwell: 2.55μs; Master gain: ch1= 1096, ch2= 928, ch3= 393; Digital gain: ch1 = 1.20, ch2 = 0.61, ch3 = 1.40; Digital offset = 0.0, Pinhole = 156μm; and laser: 488nm with 10.0% strength.

Population genetic analysis:

The ELF3 CDS sequences of accessions were downloaded from the 1001 Genome-Project (http://www.1001genomes.org/). The geographical coordinates for the accessions were obtained from the SALK database (http://signal.salk.edu/atg1001/index.php). These coordinates were used to map the geographical position of the accessions using Google maps (maps.google.com) (Table 4). For sequence alignment and phylogenetic analysis, MEGA 4.0 software was used [69]. The phylogenetic relationships between the sequences were determined using the neighbor-joining (NJ) method and applying the interior-branch test [70].

Acknowledgements

We are grateful to C Darrah for the modified pPZP221 vector. We also thank B Pieper, J de Montaigu, D Staiger, A Hörger, and D Martin for comments on the manuscript. K Schneeberger and M von Korff assisted in statistical analyses.

References:

1. Graf A, Schlereth A, Stitt M, Smith AM (2010) Circadian control of carbohydrate availability for growth in Arabidopsis plants at night. Proceedings of the National Academy of Sciences of the United States of America 107: 9458-9463.
2. Haydon MJ, Bell LJ, Webb AA (2011) Interactions between plant circadian clocks and solute transport. Journal of Experimental Botany 62: 2333-2348.
3. Sanchez A, Shin J, Davis SJ (2011) Abiotic stress and the plant circadian clock. Plant Signaling & Behavior 6: 223-231.
4. Sanchez-Villarreal A, Shin J, Bujdoso N, Obata T, Neumann U, et al. (2013) TIME FOR COFFEE is an essential component in the maintenance of metabolic homeostasis in Arabidopsis thaliana. The Plant Journal 76: 188-200.
5. Thines B, Harmon FG (2011) Four easy pieces: mechanisms underlying circadian regulation of growth and development. Current Opinion in Plant Biology 14: 31-37.
6. Dodd AN, Salathia N, Hall A, Kévei E, Tóth R, et al. (2005) Plant circadian clocks increase photosynthesis, growth, survival, and competitive advantage. Science 309: 630-633.
7. Bujdoso N, Davis SJ (2013) Mathematical modeling of an oscillating gene circuit to unravel the circadian-clock network of Arabidopsis thaliana. Frontiers in Plant Science 4:3.
8. Gendron JM, Pruneda-Paz JL, Doherty CJ, Gross AM, Kang SE, et al. (2012) Arabidopsis circadian clock protein, TOC1, is a DNA-binding transcription factor. Proceedings of the National Academy of Sciences of the United States of America 109: 3167-3172.
9. Huang W, Perez-Garcia P, Pokhilko A, Millar AJ, Antoshechkin I, et al. (2012) Mapping the core of the Arabidopsis circadian clock defines the network structure of the oscillator. Science 336: 75-79.
10. Locke JC, Kozma-Bognar L, Gould PD, Feher B, Kevei E, et al. (2006) Experimental validation of a predicted feedback loop in the multi-oscillator clock of Arabidopsis thaliana. Molecular Systems Biology 2: 59.
11. Zeilinger MN, Farre EM, Taylor SR, Kay SA, Doyle FJ (2006) A novel computational model of the circadian clock in Arabidopsis that incorporates PRR7 and PRR9. Molecular Systems Biology 2:58.
12. Chow BY, Helfer A, Nusinow DA, Kay SA (2012) ELF3 recruitment to the *PRR9* promoter requires other Evening Complex members in the Arabidopsis circadian clock. Plant Signaling and Behavior 7: 170-173.
13. Dixon LE, Knox K, Kozma-Bognar L, Southern MM, Pokhilko A, et al. (2011) Temporal repression of core circadian genes is mediated through EARLY FLOWERING 3 in Arabidopsis. Current Biology 21: 120-125.
14. Helfer A, Nusinow DA, Chow BY, Gehrke AR, Bulyk ML, et al. (2011) LUX ARRHYTHMO encodes a nighttime repressor of circadian gene expression in the Arabidopsis core clock. Current Biology 21: 126-133.
15. Herrero E, Davis SJ (2012) Time for a Nuclear Meeting: Protein Trafficking and Chromatin Dynamics Intersect in the Plant Circadian System. Molecular Plant 5: 554-65.
16. Herrero E, Kolmos E, Bujdoso N, Yuan Y, Wang M, et al. (2012) EARLY FLOWERING4 Recruitment of EARLY FLOWERING3 in the nucleus sustains the Arabidopsis circadian clock. Plant Cell 24: 428-443.
17. Kolmos E, Nowak M, Werner M, Fischer K, Schwarz G, et al. (2009) Integrating ELF4 into the circadian system through combined structural and functional studies. HFSP Journal 3: 350-366.
18. Nozue K, Covington MF, Duek PD, Lorrain S, Fankhauser C, et al. (2007) Rhythmic growth explained by coincidence between internal and external cues. Nature 448: 358-361.
19. Nusinow DA, Helfer A, Hamilton EE, King JJ, Imaizumi T, et al. (2011) The ELF4-ELF3-LUX complex links the circadian clock to diurnal control of hypocotyl growth. Nature 475: 398-402.

20. McClung CR (2011) The genetics of plant clocks. Advances in Genetics 74: 105-139.
21. McClung CR, Davis SJ (2010) Ambient thermometers in plants: from physiological outputs towards mechanisms of thermal sensing. Current Biology 20: 1086-1092.
22. Salomé PA, McClung CR (2005) PSEUDO-RESPONSE REGULATOR 7 and 9 are partially redundant genes essential for the temperature responsiveness of the Arabidopsis circadian clock. Plant Cell 17: 791-803.
23. Salome PA, Weigel D, McClung CR (2010) The role of the Arabidopsis morning loop components CCA1, LHY, PRR7, and PRR9 in temperature compensation. Plant Cell 22: 3650-3661.
24. Aschoff J (1979) Circadian Rhythms: Influences of internal and external factors on the period measured in constant conditions1. Zeitschrift für Tierpsychologie 49: 225-249.
25. Covington MF, Panda S, Liu XL, Strayer CA, Wagner DR, et al. (2001) ELF3 Modulates resetting of the circadian clock in Arabidopsis. Plant Cell 13: 1305-1316.
26. Johnson CH, Elliott JA, Foster R (2003) Entrainment of circadian programs. Chronobiology International 20: 741-774.
27. Watillon B, Kettmann R, Boxus P, Burny An (1993) Developmental and circadian pattern of rubisco activase mRNA accumulation in apple plants. Plant Molecular Biology 23: 501-509.
28. Zhong HH, Resnick AS, Straume M, Robertson McClung C (1997) Effects of synergistic signaling by phytochrome A and cryptochrome1 on circadian clock-regulated catalase expression. Plant Cell 9: 947-955.
29. David KM, Armbruster U, Tama N, Putterill J (2006) Arabidopsis GIGANTEA protein is post-transcriptionally regulated by light and dark. FEBS Letters 580: 1193-1197.
30. Liu XL, Covington MF, Fankhauser C, Chory J, Wagner DR (2001) ELF3 encodes a circadian clock-regulated nuclear protein that functions in an Arabidopsis PHYB signal transduction pathway. Plant Cell 13: 1293-1304.
31. Kolmos E, Herrero E, Bujdoso N, Millar AJ, Toth R, et al. (2011) A reduced-function allele reveals that EARLY FLOWERING3 repressive action on the circadian clock is modulated by Phytochrome signals in Arabidopsis. Plant Cell 23: 3230–3246.
32. Thines B, Harmon FG (2010) Ambient temperature response establishes ELF3 as a required component of the core Arabidopsis circadian clock. Proceedings of the National Academy of Sciences of the United States of America 107: 3257-3262.
33. Zagotta MT, Hicks KA, Jacobs CI, Young JC, Hangarter RP, et al. (1996) The Arabidopsis ELF3 gene regulates vegetative photomorphogenesis and the photoperiodic induction of flowering. The Plant Journal 10: 691-702.
34. Zagotta MT, Shannon S, Jacobs C, Meeks-Wagner DR (1992) Early-flowering mutants of Arabidopsis thaliana. Functional Plant Biology 19: 411-418.
35. Hicks KA, Millar AJ, Carré IA, Somers DE, Straume M, et al. (1996) Conditional circadian dysfunction of the Arabidopsis early-flowering 3 mutant. Science 274: 790-792.
36. Reed JW, Nagpal P, Bastow RM, Solomon KS, Dowson-Day MJ, et al. (2000) Independent action of ELF3 and phyB to control hypocotyl elongation and flowering time. Plant Physiology 122: 1149-1160.
37. Hicks KA, Albertson TM, Wagner DR (2001) EARLY FLOWERING3 encodes a novel protein that regulates circadian clock function and flowering in Arabidopsis. Plant Cell 13: 1281-1292.
38. McWatters HG, Bastow RM, Hall A, Millar AJ (2000) The ELF3 zeitnehmer regulates light signalling to the circadian clock. Nature 408: 716-720.
39. Koornneef M, Alonso-Blanco C, Vreugdenhil D (2004) Naturally occurring genetic variation in Arabidopsis thaliana. Annual Review of Plant Biology 55: 141-172.
40. Anwer MU, Davis SJ (2013) An overview of natural variation studies in the Arabidopsis thaliana circadian clock. Seminars in Cell and Developmental Biology 24: 422-429.
41. Edwards KD, Lynn JR, Gyula P, Nagy F, Millar AJ (2005) Natural Allelic Variation in the Temperature-Compensation Mechanisms of the Arabidopsis thaliana Circadian Clock. Genetics 170: 387-400.

762 **42. Swarup K, Alonso-Blanco C, Lynn JR, Michaels SD, Amasino RM, et al. (1999) Natural allelic**
763 **variation identifies new genes in the Arabidopsis circadian system. The Plant Journal 20:**
764 **67-77.**
765 **43. Michael TP, Salomé PA, Yu HJ, Spencer TR, Sharp EL, et al. (2003) Enhanced Fitness Conferred**
766 **by Naturally Occurring Variation in the Circadian Clock. Science 302: 1049-1053.**
767 **44. Boikoglou E, Ma Z, von Korff M, Davis AM, Nagy F, et al. (2011) Environmental Memory From a**
768 **Circadian Oscillator: The Arabidopsis thaliana Clock Differentially Integrates Perception of**
769 **Photic Versus Thermal Entrainment. Genetics 189: 655-664.**
770 **45. Darrah C, Taylor BL, Edwards KD, Brown PE, Hall A, et al. (2006) Analysis of phase of**
771 **LUCIFERASE expression reveals novel circadian quantitative trait loci in Arabidopsis. Plant**
772 **Physiology 140: 1464-1474.**
773 **46. Loudet O, Chaillou S, Camilleri C, Bouchez D, Daniel-Vedele F (2002) Bay-0 x Shahdara**
774 **recombinant inbred line population: a powerful tool for the genetic dissection of complex**
775 **traits in Arabidopsis. Theoretical and Applied Genetics 104: 1173-1184.**
776 **47. Coluccio MP, Sanchez SE, Kasulin L, Yanovsky MJ, Botto JF (2011) Genetic mapping of natural**
777 **variation in a shade avoidance response: ELF3 is the candidate gene for a QTL in hypocotyl**
778 **growth regulation. Journal of Experimental Botany 62: 167-176.**
779 **48. Tajima T, Oda A, Nakagawa M, Kamada H, Mizoguchi T (2007) Natural variation of**
780 **polyglutamine repeats of a circadian clock gene ELF3 in Arabidopsis. Plant Biotechnology**
781 **24: 237-240.**
782 **49. Jimenez-Gomez JM, Wallace AD, Maloof JN (2010) Network analysis identifies ELF3 as a QTL for**
783 **the shade avoidance response in Arabidopsis. PLoS Genetics 6.**
784 **50. Fowler S, Lee K, Onouchi H, Samach A, Richardson K, et al. (1999) GIGANTEA: a circadian clock-**
785 **controlled gene that regulates photoperiodic flowering in Arabidopsis and encodes a**
786 **protein with several possible membrane-spanning domains. The EMBO Journal 18: 4679-**
787 **4688.**
788 **51. Kikis EA, Khanna R, Quail PH (2005) ELF4 is a phytochrome-regulated component of a negative-**
789 **feedback loop involving the central oscillator components CCA1 and LHY. The Plant Journal**
790 **44: 300-313.**
791 **52. Yu JW, Rubio V, Lee NY, Bai S, Lee SY, et al. (2008) COP1 and ELF3 control circadian function and**
792 **photoperiodic flowering by regulating GI stability. Molecular Cell 32: 617-630.**
793 **53. Farre EM, Harmer SL, Harmon FG, Yanovsky MJ, Kay SA (2005) Overlapping and distinct roles of**
794 **PRR7 and PRR9 in the Arabidopsis circadian clock. Current Biology 15: 47-54.**
795 **54. Nakamichi N, Kiba T, Henriques R, Mizuno T, Chua NH, et al. (2010) PSEUDO-RESPONSE**
796 **REGULATORS 9, 7, and 5 are transcriptional repressors in the Arabidopsis circadian clock.**
797 **Plant Cell 22: 594-605.**
798 **55. Ding Z, Doyle MR, Amasino RM, Davis SJ (2007) A complex genetic interaction between**
799 **Arabidopsis thaliana TOC1 and CCA1/LHY in driving the circadian clock and in output**
800 **regulation. Genetics 176: 1501-1510.**
801 **56. Chen M, Galvão RM, Li M, Burger B, Bugea J, et al. (2010) Arabidopsis HEMERA/pTAC12**
802 **Initiates Photomorphogenesis by Phytochromes. Cell 141: 1230-1240.**
803 **57. Mas P, Devlin PF, Panda S, Kay SA (2000) Functional interaction of phytochrome B and**
804 **cryptochrome 2. Nature 408: 207-211.**
805 **58. Kim Y, Lim J, Yeom M, Kim H, Kim J, et al (2013) ELF4 regulates GIGANTEA chromatin access**
806 **through subnuclear sequestration. Cell Reports 3: 671-677.**
807 **59. Huang X, Effgen S, Meyer RC, Theres K, Koornneef M (2012) Epistatic Natural Allelic Variation**
808 **Reveals a Function of AGAMOUS-LIKE6 in Axillary Bud Formation in Arabidopsis. Plant Cell**
809 **24: 2364-2379.**
810 **60. Méndez-Vigo B, Martínez-Zapater JM, Alonso-Blanco C (2013) The Flowering Repressor SVP**
811 **Underlies a Novel Arabidopsis thaliana QTL Interacting with the Genetic Background. PLoS**
812 **Genetics 9: e1003289.**

61. Sugliani M, Rajjou L, Clerkx EJ, Koornneef M, Soppe WJ (2009) Natural modifiers of seed longevity in the Arabidopsis mutants abscisic acid insensitive3-5 (abi3-5) and leafy cotyledon1-3 (lec1-3). New Phytologist 184: 898-908.

62. Undurraga SF, Press MO, Legendre M, Bujdoso N, Bale J, et al. (2012) Background-dependent effects of polyglutamine variation in the Arabidopsis thaliana gene ELF3. Proceedings of the National Academy of Sciences of the United States of America 109: 47 19363-19367.

63. Davis A, Hall A, Millar A, Darrah C, Davis S (2009) Protocol: Streamlined sub-protocols for floral-dip transformation and selection of transformants in Arabidopsis thaliana. Plant Methods 5: 3.

64. Hanano S, Domagalska MA, Nagy F, Davis SJ (2006) Multiple phytohormones influence distinct parameters of the plant circadian clock. Genes Cells 11: 1381-1392.

65. Hanano S, Stracke R, Jakoby M, Merkle T, Domagalska MA, et al. (2008) A systematic survey in Arabidopsis thaliana of transcription factors that modulate circadian parameters. BMC Genomics 9: 182.

66. Davis SJ, Bhoo SH, Durski AM, Walker JM, Vierstra RD (2001) The Heme-Oxygenase Family Required for Phytochrome Chromophore Biosynthesis Is Necessary for Proper Photomorphogenesis in Higher Plants. Plant Physiology 126: 656-669.

67. Domagalska MA, Sarnowska E, Nagy F, Davis SJ (2010) Genetic analyses of interactions among gibberellin, abscisic acid, and brassinosteroids in the control of flowering time in Arabidopsis thaliana. PLoS One 5: e14012.

68. Keurentjes JJB, Bentsink L, Alonso-Blanco C, Hanhart CJ, Blankestijn-De Vries H, et al. (2007) Development of a near-isogenic line population of Arabidopsis thaliana and comparison of mapping power with a recombinant inbred line population. Genetics 175: 891-905.

69. Tamura K, Dudley J, Nei M, Kumar S (2007) MEGA4: Molecular Evolutionary Genetics Analysis (MEGA) Software Version 4.0. Molecular Biology and Evolution 24: 1596-1599.

70. Saitou N, Nei M (1987) The neighbor-joining method: a new method for reconstructing phylogenetic trees. Molecular Biology and Evolution 4: 406-425.

Figure Legends:

Figure 1. Illustrative and statistical features of *CCR2* periodicity post-photic versus post- thermal entrainment in BxS populations.

(A) Normal frequency distribution of *CCR2* periodicity in BxS individuals. Blue-colored bars represent periodicity after photic entrainment, and magenta-colored bars represent periodicity after thermal entrainment. Bay-0 and Sha denote the periodicity of *CCR2* in the parental genotypes. Note the skew of temperature-entrained plants to shorter periodicity, when compared to photic-entrained plants. (B) Periodicity differences of *CCR2* in BxS RIL lines. The x-axis denotes 54 RILs of which periodicity was assayed in both in LD and TMP entrainment (see Supplementary File 1 and Supplementary File 2). The y-axis represents the periodicity differences of thermal minus photic-entrained lines (calculated as $Period_{LD}$ – $Period_{TMP}$). (C) A scatter plot for TMP vs. LD periodicities from the BxS RILs described in the tables Supplementary File 1 and Supplementary File 2.

Figure 2. Map-based cloning identifies *ELF3* as a candidate for chr2 QTL.

Period estimates of *CCR2::LUC* expression in (A) three independent HIFs (57, 92, and 343) harboring either the Bay-0 or the Sha allele at QTL confidence interval (B) parental accessions and NIL-S with introgression of Sha at QTL confidence interval in otherwise homogeneous Bay-0 background, under LL and in DD. (C) Schematic diagram showing the fine mapping strategy of chr2 locus. Black and grey bars represent Bay-0 and Sha genotypes, respectively. The names below the bars represent the molecular markers used for genotyping, and the numbers above correspond to their physical position on the genome. The crosses represent the position of the recombination event. Two recombinants, 89-S and 539-B, were found to have a recombination event surrounding a 40KB region, where 9 annotated genes are located, as indicated below the solid bar. (D) Free-running profile of *CCR2::LUC* expression in recombinants 89-S, 539-B and Bay-0 under continuous red and blue light (LL). (E) Period estimates of rhythm shown in (D). All error bars indicate SEM, where $n \geq 24$. Mean values that are significantly different from Bay-0 wild type are indicated by *, **, or *** for P-values (ANOVA) < 0.05, 0.01, or 0.001, respectively.

Figure 3. Transgenic complementation confirms ELF3 as QTG underlying Chr2 QTL.

Free-running profile of *CCR2::LUC* expression in Bay-0, Sha, and NIL in darkness (A), Left y-axis shows the luminescence measures of Bay and NIL, and the right y-axis shows the

luminescence measures of Sha. NIL with introgression of Sha at *ELF3* could not sustain the robust rhythms of *CCR2::LUC* after four days in darkness. Error bars represent SEM, n ≥ 24. (B) Free-running period estimates of *CCR2::LUC* and *LHY::LUC* expression in T2 transgenic lines harboring either *ELF3-Bay-YFP* or *ELF3-Sha-YFP* in Ws-2 background. The data are the average of three independent, single-insert lines displaying similar rhythm profile. Error bars represent SEM, n = 96. (C) Sequence comparison of *ELF3-Bay* and *ELF3-Sha*. Schematic representation of *ELF3* (AT2G25930). Vertical bars show the position of the nucleic acid transition. The letters above the bars represent the nucleic acid in Bay, and letters below represent the nucleic acid in Sha. The numbers above the letters represent the position of the nonsynonymous change. The letters in parenthesis show the amino-acid change.

Figure 4. Flowering time and hypocotyl length measurements for *ELF3-Sha*.

(A) Flowering time of HIF 89-S, HIF 539-B, NIL, and Bay-0 under long day (16L:8D) and short day (8L:16D). The flowering time was counted as the number of days at the appearance of 1cm bolt. (B) Hypocotyl length of HIF 89-S, HIF 539-B, NIL, *elf3-1*, Sha, and Bay-0 under short day (8L:16D), under RR (15 µmol m-2s-1), and under BB (15 µmol m-2s-1). Error bars represent the standard deviation. Significance as described in Figure 2 compared to Bay-0, except HIF 89-S, which was compared to HIF 539-B.

Figure 5. Molecular basis of *ELF3-Sha* phenotypes

(A) Schematic diagram explaining the different promoter-coding combinations used in (B). The Sha promoter of *ELF3* fused with different coding regions is shown (for details see Materials and Methods). The encoded amino-acid residue at position 362, along with the number of encoded glutamines, is shown. (B) Period estimates of the *LHY::LUC* expression in the lines explained in (A). Note that the lines SpSc and SpBa2v with Valine in the coding part displayed period acceleration, irrespective of the number of glutamines. Error bars represent SEM, n = 48. Significance as explained in Figure 2, compared to *SpBc*. Free-running profile of *LHY::LUC* expression in T2 transgenic lines harboring either *ELF3-Bay* or *ELF3-A362V* in Ws-2 genetic background under LL (C) and in DD (D). A single nucleotide exchange was induced in *ELF3-Bay* to change the encoded alanine residue at position 362 to valine (*ELF3-A362V*). The data are the average of three independent single-insert lines with similar rhythm profile. (E) Period estimates of the lines shown in (C) and (D). Error bars represent SEM, n = 96. Mean values that are significantly different from Bay-0 wild type are indicated by *, **, or *** for P-values (ANOVA) < 0.05, 0.01, or 0.001, respectively.

Figure 6. Alterations in the *ELF3-Sha* oscillator and clock resetting

(A) Free-running profile of *LHY::LUC* expression in *ELF3-Bay* and *ELF3-A362V* in a 15-day continuous experiment under consecutive light and in dark conditions. The plants were entrained for 7 days under 12h:12h light dark cycles, followed by transfer to LL and measurement of *LHY::LUC* expression for 6 days. On day 7, plants were transferred to darkness, and the measurement of *LHY::LUC* was continued in DD for four more days. On day 11, the plants were transferred to light conditions again, and the expression profile of *LHY::LUC* was measured for an additional four days. Open bars in the graph represent time in LL, and closed bar represents time in DD. Error bars represent SEM and are shown on every third reading. (B) Period and R.A.E. analysis of profiles shown in (A) n=48. (C) Phase shifts in dark-adapted seedlings after resumption to LL. *ELF3-Bay* and *ELF3-A362V* plants entrained for 7 days under light/dark cycles (LD) were transferred in DD for one day and then replicate samples were released into LL at 4-h intervals, monitoring the phase of *LHY* expression in LL to determine the state of the oscillator in the preceding DD interval. Phase difference plot (Phase ELF3-Bay - ELF3-A362V) for three days in DD is shown. Third peak under LL was used for phase analysis. n=36. Experiment was repeated three times with similar results. (D) Frequency demultiplication assay. After 7 days of entrainment under 12L:12D (T=24) cycles, the *LHY:LUC* profile was monitored under 12L:12D (T=24) for one day and then 6L:6D (T=12) for 4 days. The shaded boxes indicate the duration of the LD cycles. For clarification, the *LHY::LUC* profiles from day-3 to day-5 is magnified and shown below.

Figure 7. Alanine sustains robust oscillator in darkness.

(A-C) Scatter plot for R.A.E. against period showing estimates of individual *ELF3-Bay* and *ELF3-A362V* lines shown in (Figure 5A). Only lines with R.A.E.<1.0 were plotted.

Figure 8. Circadian oscillator does not abolish in *ELF3-Sha* in darkness.

(A) Phase shifts in dark-adapted seedlings after resumption to LL. *ELF3-Bay* and *ELF3-A362V* plants entrained for 7 days under light/dark cycles (LD) were transferred in DD for one day and then replicate samples were released into LL at 4-h intervals, monitoring the phase of *LHY* expression in LL to determine the state of the oscillator in the preceding DD interval. Phase was calculated relative to dawn (ZT00), n=36. (B) The *LHY::LUC* profile in *ELF3-Bay* and *ELF3-A362V* after 128h in darkness. Note the robust rhythms of *LHY::LUC* in both lines.

Figure 9. *ELF3-Sha* is short-period under a range of light intensities

Free-running period of Bay and NIL-S under different intensities of (A) red (B) blue and (C) red+blue lights (~3:1). Plants were entrained for 7 days under 12h LD cycles (white light) before transferring to the respective light conditions. Neutral density filters were used to control the light intensities. Light intensities were measured in μmol $m^{-2}s^{-1}$ and were transformed to log10 scale shown in the graphs. DD represents darkness. Error bars represent SEM, n = 36.

Figure 10. Compromised clock network in *ELF3-Sha*

Luciferase expression profile of different clock genes in NIL, *elf3-1*, *elf3-4* and Bay-0 under LL (left panel, A-F) and in DD (right panel, G-L). (A,G) *CCA1::LUC* (B,H) *LHY::LUC* (C,I) *TOC1::LUC* (D,J) *GI::LUC* (E,K) *PRR7::LUC* and, (F,L) *PRR9::LUC*. Error bars represent SEM and are shown on every third reading. Note that the NIL-S displayed an intermediate expression of all clock genes relative to the null mutants *elf3-1* and *elf3-4* compared to Bay-0.

Figure 11. Transcript accumulation pattern of different clock genes under LL.

Transcript accumulation of different clock genes in Bay-0, Sha, NIL-S and *elf3-4* under LL. (A) *CCA1::LUC* (B) *LHY::LUC* (C) *PRR7::LUC* and (D) *PRR9::LUC,* (E) *GI::LUC* and (F) *TOC1::LUC*. Error bars represent the standard deviation of three technical repeats. Expression levels are normalized for *PROTEIN 19 PHOSPHATASE 2a subunit A3* (*PP2A*). Growth conditions, quantitative RT-PCR, and primer sequences were previously described [17,31].

Figure 12. Sub-cellular localization defects of ELF3-Sha

(A) and (B) show maximum intensity projection of ELF3-YFP localization in root cells of ELF3-Bay-YFP (A) and ELF3-Sha-YFP (B). Arrows indicate the nuclei that are magnified four times and shown in small boxes at the bottom of (A) and (B). Note that ELF3 forms distinct nuclear foci in ELF3-Bay, whereas in ELF3-Sha, YFP signal for ELF3 is diffused in the nucleus. Scale bar is 20μm. (C) and (D) display the YFP intensity distribution of (A) and (B) in visual-thermal units, respectively. Note that the ELF3 cytoplasmic contents were higher in ELF3-Sha as compared to ELF3-Bay. (E) shows the nucleus-to-cytoplasmic fluorescence ratio of ELF3-Bay-YFP and ELF3-Sha-YFP, as calculated by Image J. Error bars represent

S.E.M., n=3. Significance as described in Figure 2. The representative data of three independent experiments and three independent lines are shown.

Figure 13. ELF3 cyclic accumulation is altered in *ELF3-Sha*

Accumulation pattern of *ELF3* transcript and protein in *ELF3-Bay*-YFP and *ELF3-Sha*-YFP lines under LD (A,B), LL (C,D) and in DD (E,F). For LD, plants were grown under 12L:12D cycles for 6 days, and starting the next day at ZT0, plants were harvested every four hours for RNA extraction and then, separately, scanned under the microscope for cellular studies. For LL and DD, after initial entrainment, plants were transferred under white light or in darkness for one day, followed by harvesting the samples for RNA extraction or taking pictures for their respective *zeitgeber* time. This microscopic experiment was performed three times with similar results.

Figure 14. Distribution of the *ELF3* locus

(A) Neighbor-joining tree showing the phylogenetic relationship of *ELF3* coding sequence of 251 accessions. All accessions harboring *ELF3-Sha* allele were grouped in a single clade indicated by red-filled circles. Scale represents the distance calculated by interior-branch test. Sites with gaps/missing data were not included in the analysis (B) Geographical distribution of *ELF3-Sha* allele. Accessions harboring *ELF3-Sha* are shown with pink marks, whereas blue marks represent *ELF3-Bay* allele. Locations of Bay and Sha are shown with yellow and green marks, respectively.

Supplementary File 1

RIL periodicity of *CCR2::LUC* in BxS after photic entrainment

Supplementary File 2
RIL periodicity of *CCR2::LUC* in BxS after thermal entrainment

Supplementary File 3
Detail of primers used

Table 1

Circadian periodicity analysis of the BxS RILs after photic or thermal entrainment

	Zeitgeber	Mean[a]	S. E	95% Confidence Interval	
				Lower Bound	Upper Bound
BxS	LD	26.702	0.035	26.633	26.771
	TMP	26.269	0.034	26.202	26.335

LD-TMP		BxS
Pairwise comparisons	Mean difference (hours)	0.433
	S. E	0.047
	Significance	<0.001
Correlations	Correlation coefficient	0.86
	Significance	0.001

LD stands for photic-*zeitgeber* and TMP for thermal-*zeitgeber*

[a] denotes the modified population marginal mean for the 95% Confidence Interval

S.E. denotes standard error

LD-TMP denotes the pairwise comparisons such that TMP period is subtracted from LD period

Table 2

Statistical analysis of *CCR2* circadian periodicity after the two *zeitgeber* protocols for BxS population

Overall model	Univariate BxS	
Factor	**F**	**P**
Genotype	7.753	<0.001
Environment	36.413	<0.001
Environment*Genotype	2.183	<0.001

		Univariate LD		CV LD	Univariate TMP		CV TMP
		F	**P**		**F**	**P**	
BxS	**RIL**	10.387	<0.001	18.043	7.382	<0.001	16.498
	TRANS (RIL)	1.513	<0.001		1.915	<0.001	

F = mean sum of squares\error sum of squares. P = significance value of the F-ratio

Genotype denotes RIL, ENVIRONMENT denotes the different entrainments, TRANS denotes independent transformants of each genotype

*denotes the testing of an interaction between two factors, whereas B(A) denotes the testing main factor A in which a factor B is nested

CV is the coefficient of genetic variation, LD stands for photic and TMP stands for thermal entrainment

NS denotes nonsignificance

Table 3

Localization of the main QTLs for the BxS population after photic versus thermal *zeitgeber* protocols

Zeitgeber	h^2	Chromosome	Position (cM)	LOD score (*)	%expl variance	F	P Value	2a (h)
LD	0.76	I	63.7	3.21	14.9	7.704	0.007	-0.614
		II	34.5	5.72	27.3	20.784	<0.001	1.003
		IV	69.9	3.89	17.1	14.003	<0.001	0.833
TMP	0.73	II	34.5	4.56	25.5	25.033	<0.001	0.988
		IV	69.9	3.26	16.2	6.501	0.014	0.508

H^2 denotes broad sense heritability

(cM) denotes centiMorgan

(*) LOD- score threshold was determined at 2.4

% expl variance is the percent of explained variance

F = mean sum of squares\error sum of squares **P** denotes the significance value of the F-ratio

2a denotes the additive effect of Bay allele when the effect of the Sha allele on period is subtracted

(h) denotes the effect in hours

- denotes that the Sha allele displayed longer period than that of Bay allele

Table 4

Geographical location of the 15 accessions with *ELF3-Sha* allele

Abbreviation	Name	Stock ID	Country	Location	Latitude	Longitude	Altitude
ICE130	Kolyvan/Kly-4	CS76384	Russia	Kolyvan	51.32	82.55	505
ICE138	Lebjashje/Leb-3	CS76426	Russia	Altaijskij Kraj	51.65	80.82	301
ICE70	Borskoje/Borsk-2	CS76421	Russia	Samarskaja Oblast	53.04	51.75	75
ICE71	Shiguljovsk/Shigu-1	CS76375	Russia	Samarskaja Oblast	53.33	49.48	181
ICE72	Shiguljovsk/Shigu-2	CS76374	Russia	Samarskaja Oblast	53.33	49.48	181
Kar1	Karakol	CS76522	Kyrgyzstan	Susamyr village / West Karakol river	42.3	74.36	2503
Kondara	Kondara	CS76532	Tadjikistan	Khurmatov	38.5	68.5	815
Kz9	Kazakhstan	CS76537	Kazakhstan	Karagandy	49.67	73.33	535
Nemrut	Nemrut-1	CS76398	Turkey	Nemrut Dag	38.64	42.23	2249
Neo6	Neo6	CS76560	Tajikistan	Jawshangoz village	37.35	72.46	3467
Rubenzhoe	Rubenzhoe-1	CS76594	Ukraine	Rubezhnoe	49.01	38.36	56
Sha	Shakdara	CS76382	Tadjikistan	Pamiro-Alay	38.90	69.05	3439
Sorbo	Sorbo	CS22653	Tadjikistan		38.82	69.48	1751
Westkar4	West Karakol	CS76629	Kyrgyzstan	Karakol valley	42.3	74	2187
Zal1	Zal1	CS76634	Kyrgyzstan	Tchong-Kemin valley / Djachyl-Kul lake	42.8	76.35	2230

A

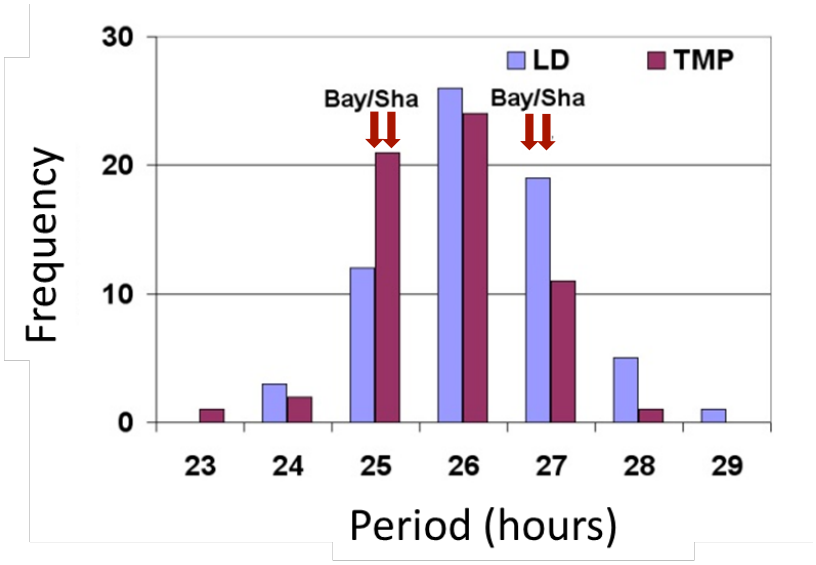
30
20
10
0
LD
TMP
Bay/Sha
Bay/Sha
Frequency
23
24
25
26
27
28
29
Period (hours)

B

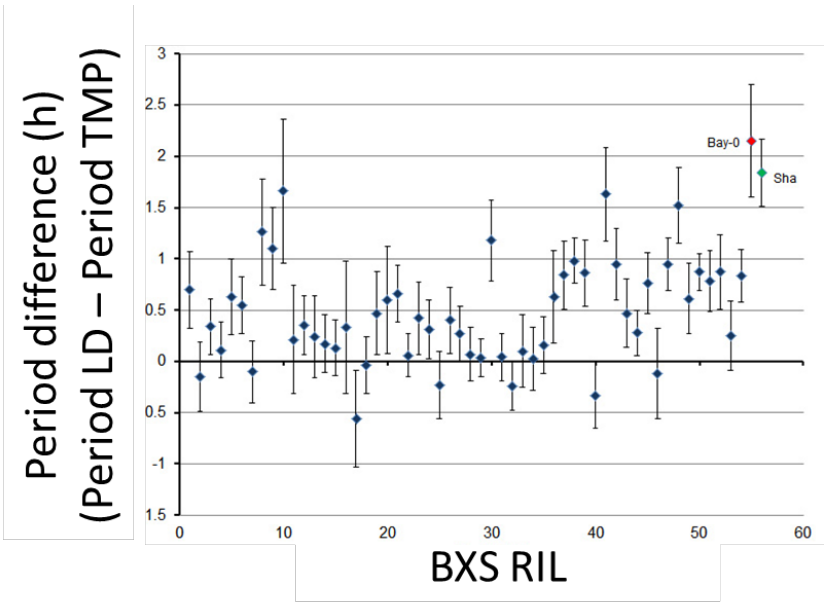
Period difference (h)
(Period LD – Period TMP)
3
2.5
2
1.5
1
0.5
0
0.5
-1
1.5
Bay-0
Sha
0
10
20
30
40
50
60
BXS RIL

C

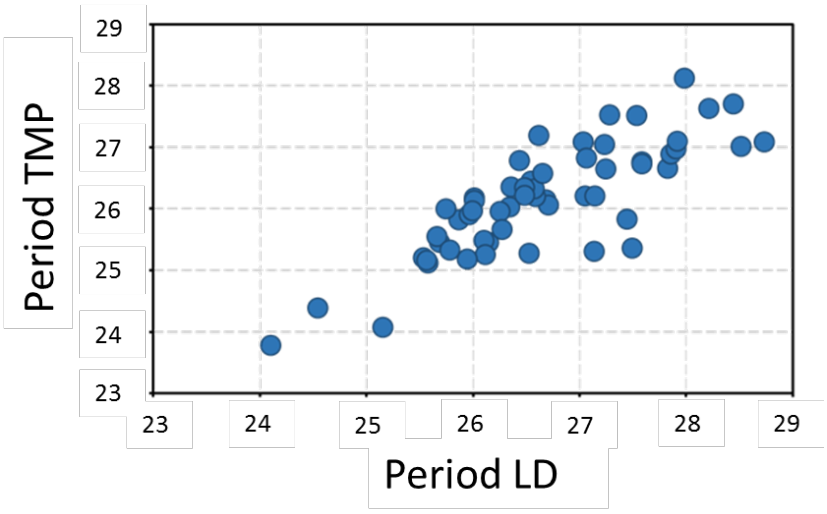
Period TMP
29
28
27
26
25
24
23
23
24
25
26
27
28
29
Period LD

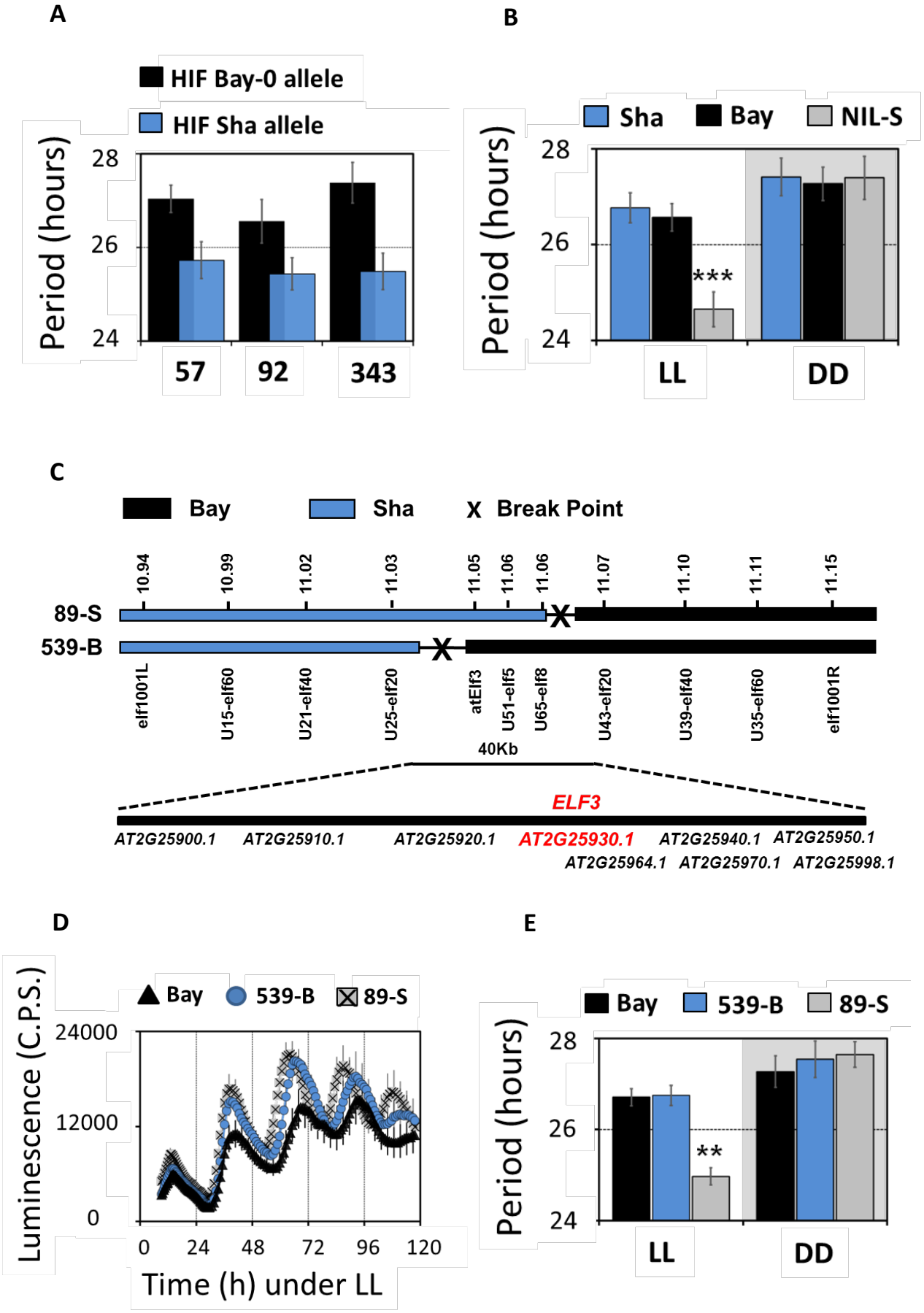
A
HIF Bay-0 allele
HIF Sha allele
Period (hours)
28
26
24
57
92
343
B
Sha
Bay
NIL-S
Period (hours)
28
26
24
***
LL
DD
C
Bay
Sha
X Break Point
10.94
10.99
11.02
11.03
11.05
11.06
11.06
11.07
11.10
11.11
11.15
89-S
539-B
elf1001L
U15-elf60
U21-elf40
U25-elf20
atElf3
U51-elf5
U65-elf8
U43-elf20
U39-elf40
U35-elf60
elf1001R
40Kb
ELF3
AT2G25900.1
AT2G25910.1
AT2G25920.1
AT2G25930.1
AT2G25940.1
AT2G25950.1
AT2G25964.1
AT2G25970.1
AT2G25998.1
D
Bay
539-B
89-S
Luminescence (C.P.S.)
24000
12000
0
0
24
48
72
96
120
Time (h) under LL
E
Bay
539-B
89-S
Period (hours)
28
26
24
**
LL
DD

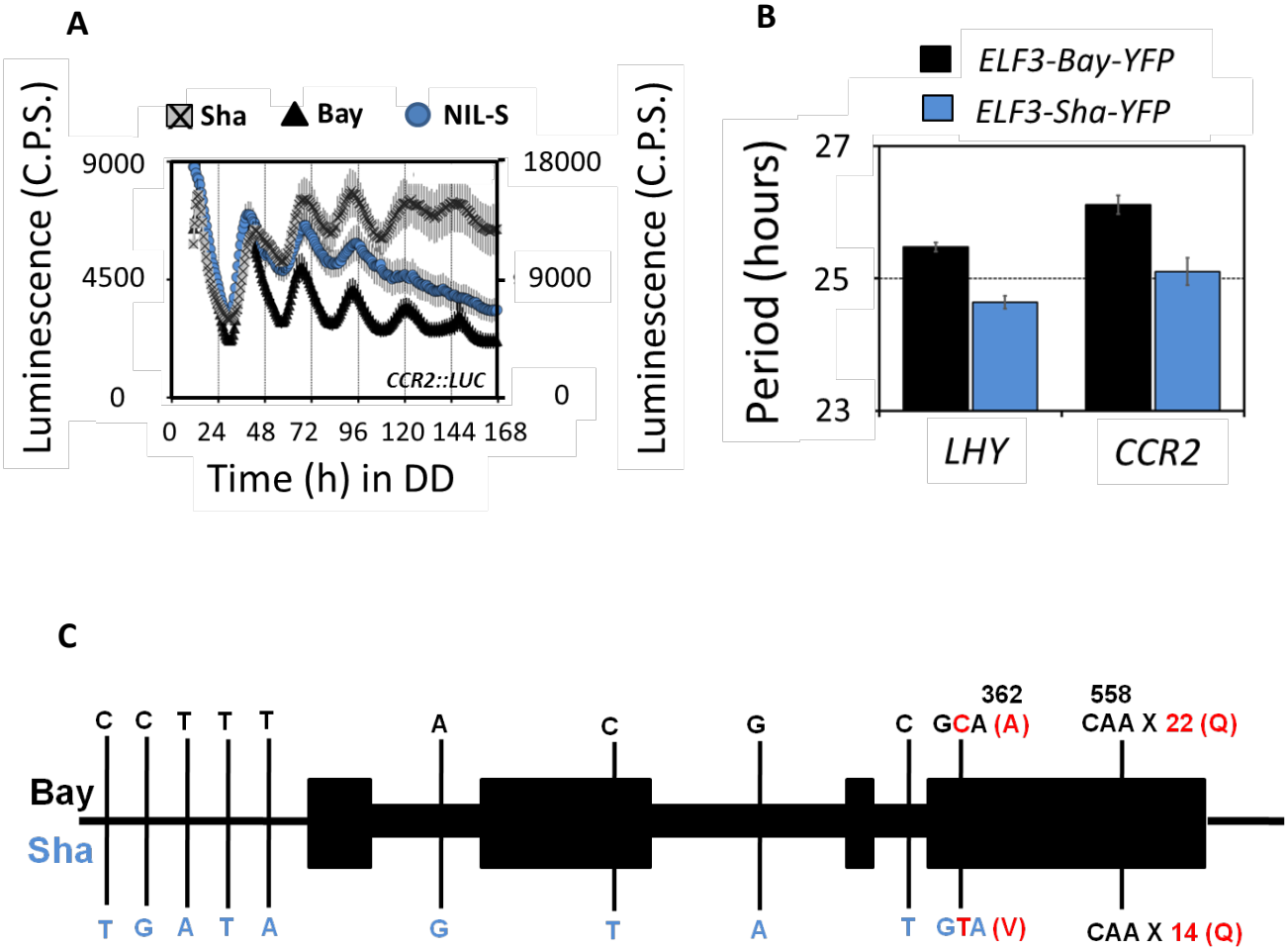
A
Sha
Bay
NIL-S
9000
4500
0
18000
9000
0
CCR2::LUC
0 24 48 72 96 120 144 168
Time (h) in DD
Luminescence (C.P.S.)
Luminescence (C.P.S.)
B
ELF3-Bay-YFP
ELF3-Sha-YFP
Period (hours)
27
25
23
LHY
CCR2
C
C C T T T
A
C
G
C GCA (A)
362
558
CAA X 22 (Q)
Bay
Sha
T G A T A
G
T
A
T GTA (V)
CAA X 14 (Q)

A

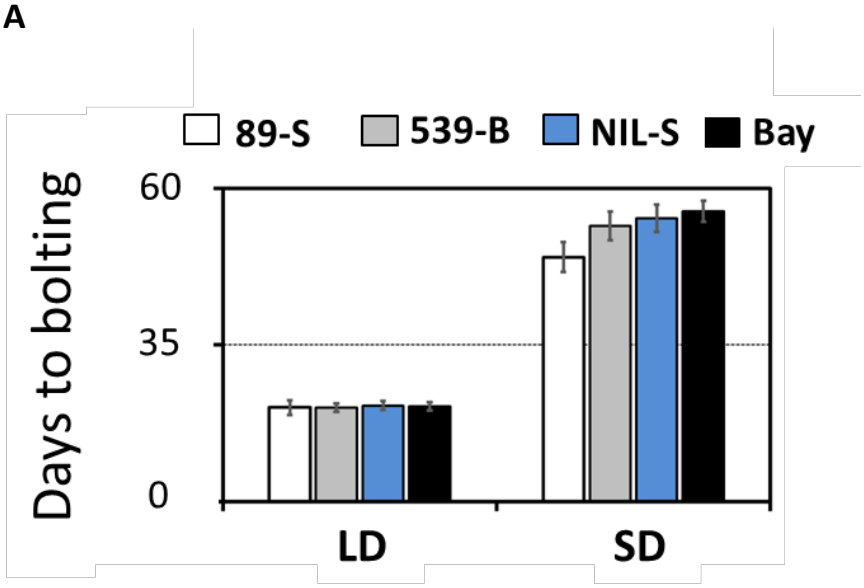
89-S
539-B
NIL-S
Bay
Days to bolting
60
35
0
LD
SD

B

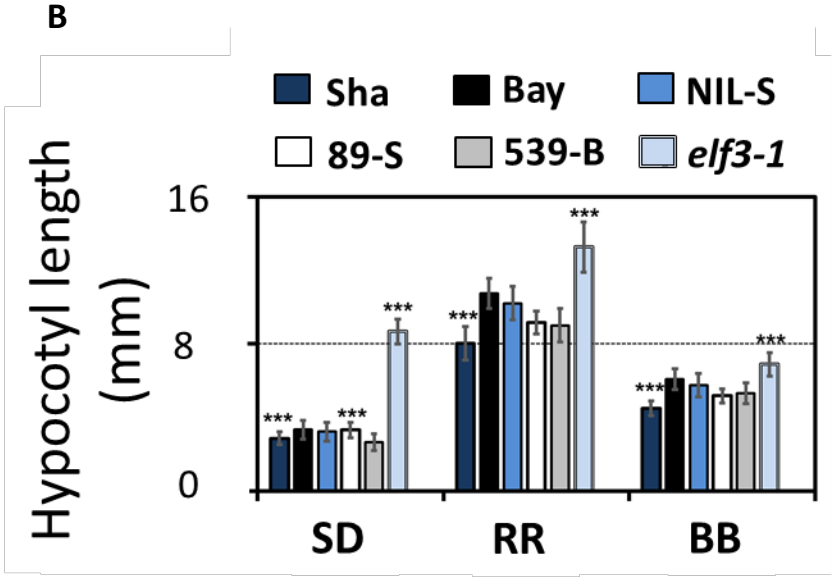
Sha
Bay
NIL-S
89-S
539-B
elf3-1
Hypocotyl length (mm)
16
8
0
***
SD
RR
BB

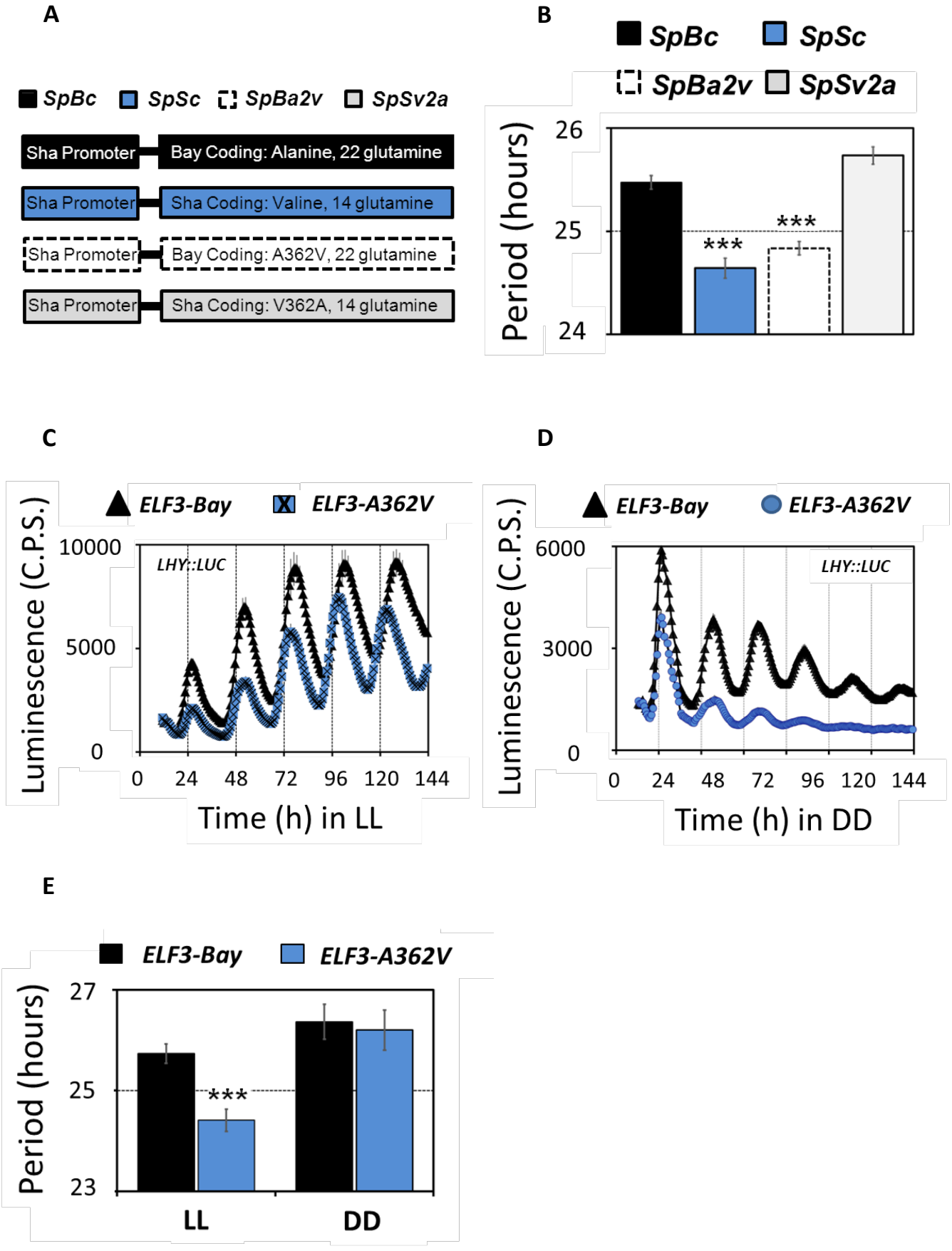
A
SpBc
SpSc
SpBa2v
SpSv2a
Sha Promoter
Bay Coding: Alanine, 22 glutamine
Sha Promoter
Sha Coding: Valine, 14 glutamine
Sha Promoter
Bay Coding: A362V, 22 glutamine
Sha Promoter
Sha Coding: V362A, 14 glutamine
B
SpBc
SpSc
SpBa2v
SpSv2a
Period (hours)
26
25
24
***
***
C
ELF3-Bay
ELF3-A362V
Luminescence (C.P.S.)
10000
5000
0
LHY::LUC
0
24
48
72
96
120
144
Time (h) in LL
D
ELF3-Bay
ELF3-A362V
Luminescence (C.P.S.)
6000
3000
0
LHY::LUC
0
24
48
72
96
120
144
Time (h) in DD
E
ELF3-Bay
ELF3-A362V
Period (hours)
27
25
23
***
LL
DD

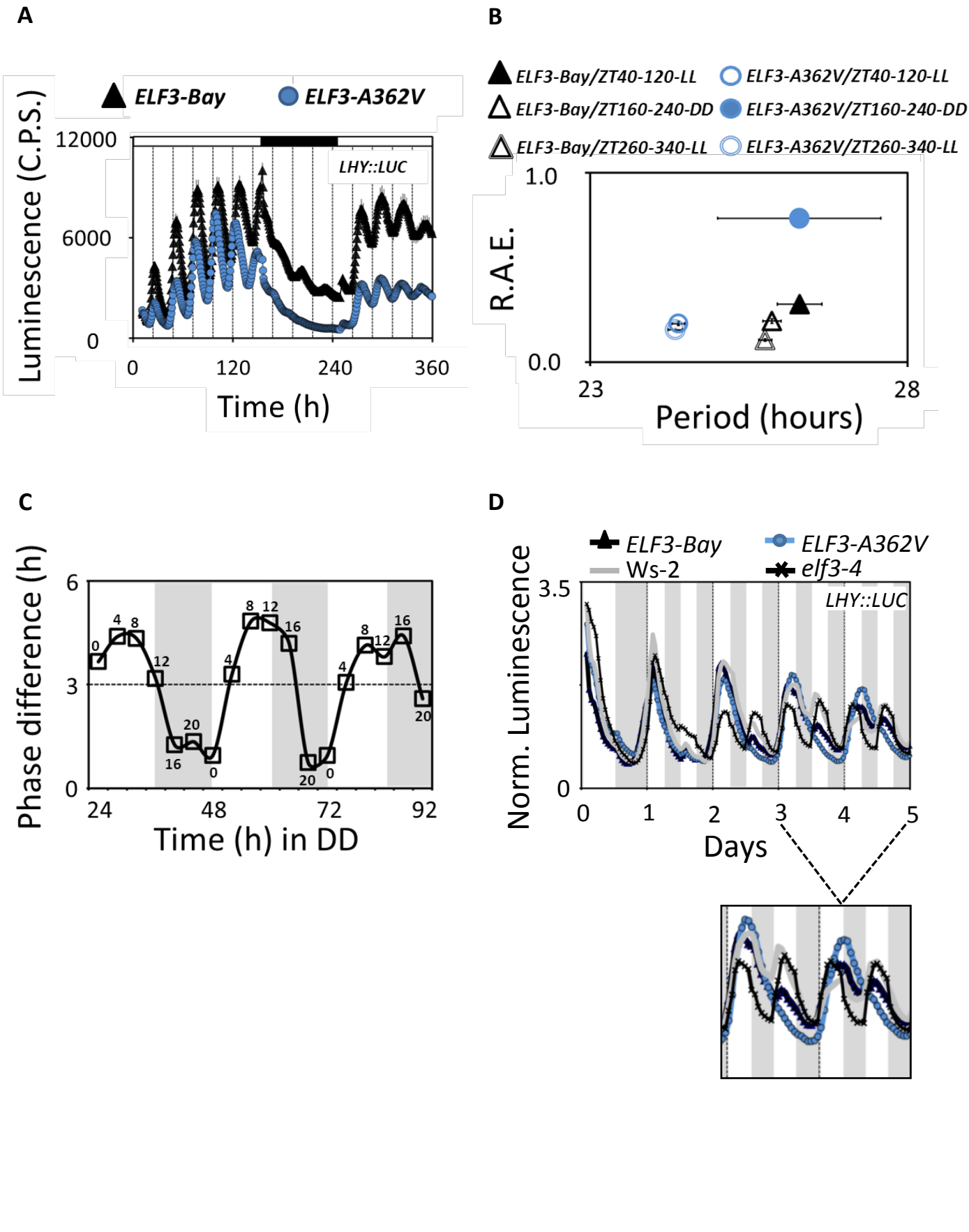
A
ELF3-Bay
ELF3-A362V
LHY::LUC
Luminescence (C.P.S.)
12000
6000
0
0
120
240
360
Time (h)
B
ELF3-Bay/ZT40-120-LL
ELF3-A362V/ZT40-120-LL
ELF3-Bay/ZT160-240-DD
ELF3-A362V/ZT160-240-DD
ELF3-Bay/ZT260-340-LL
ELF3-A362V/ZT260-340-LL
R.A.E.
1.0
0.0
23
28
Period (hours)
C
Phase difference (h)
6
3
0
24
48
72
92
Time (h) in DD
D
ELF3-Bay
Ws-2
ELF3-A362V
elf3-4
LHY::LUC
Norm. Luminescence
3.5
0
0
1
2
3
4
5
Days

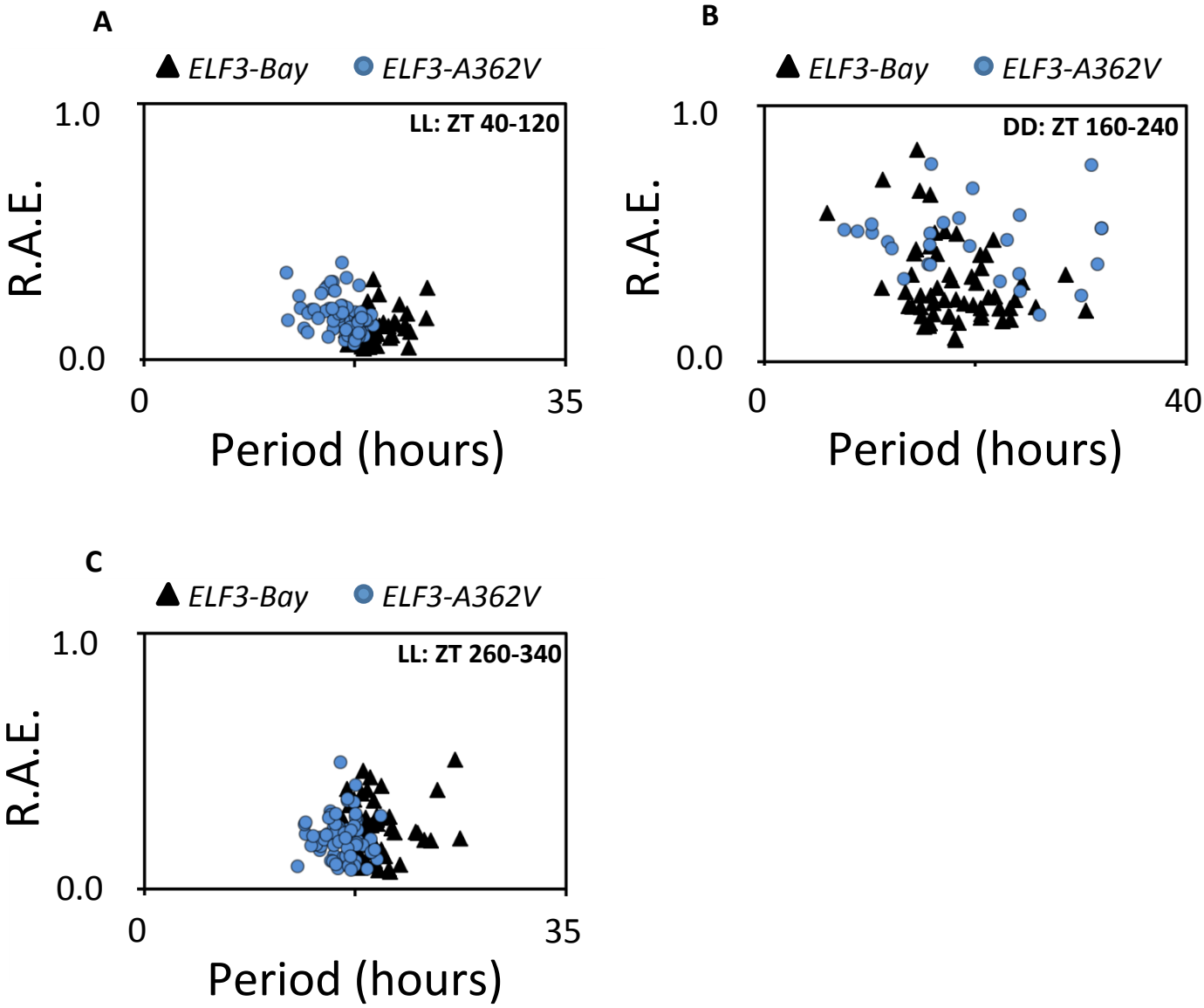
A
ELF3-Bay
ELF3-A362V
LL: ZT 40-120
1.0
0.0
R.A.E.
0
35
Period (hours)
B
ELF3-Bay
ELF3-A362V
DD: ZT 160-240
1.0
0.0
R.A.E.
0
40
Period (hours)
C
ELF3-Bay
ELF3-A362V
LL: ZT 260-340
1.0
0.0
R.A.E.
0
35
Period (hours)

A

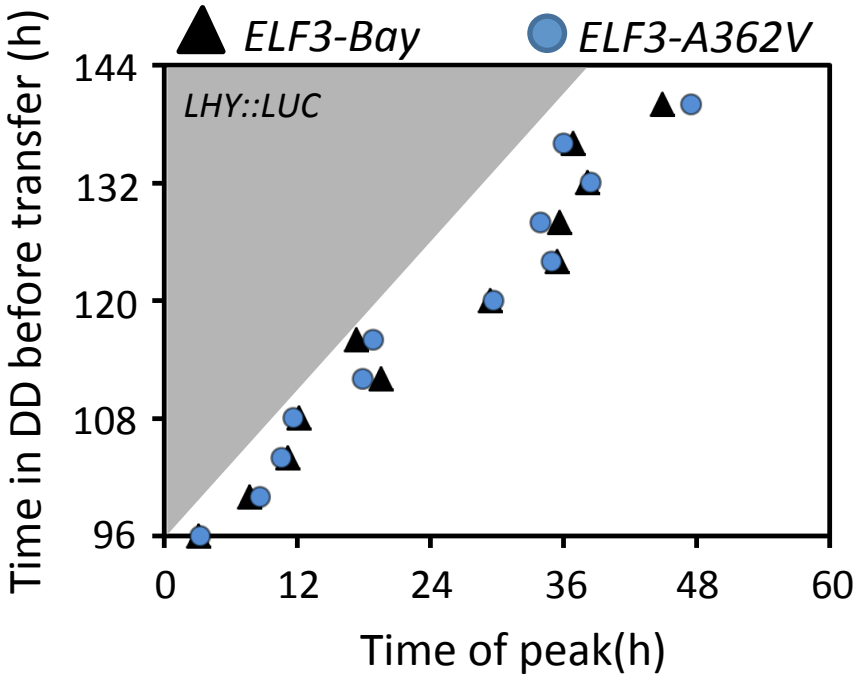
ELF3-Bay
ELF3-A362V
LHY::LUC
Time in DD before transfer (h)
144
132
120
108
96
0
12
24
36
48
60
Time of peak(h)

B

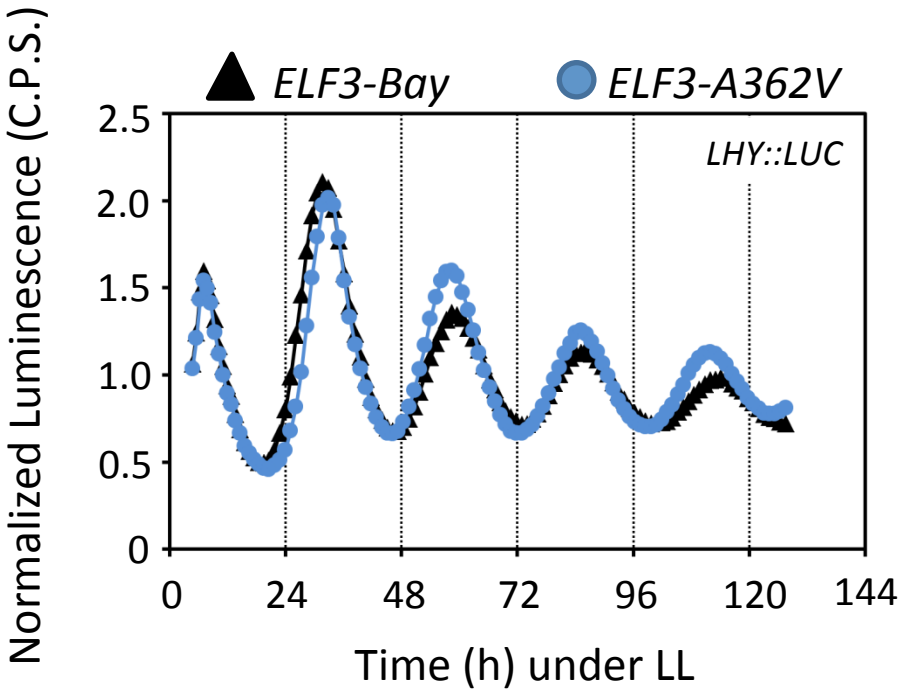
ELF3-Bay
ELF3-A362V
LHY::LUC
Normalized Luminescence (C.P.S.)
2.5
2.0
1.5
1.0
0.5
0
0
24
48
72
96
120
144
Time (h) under LL

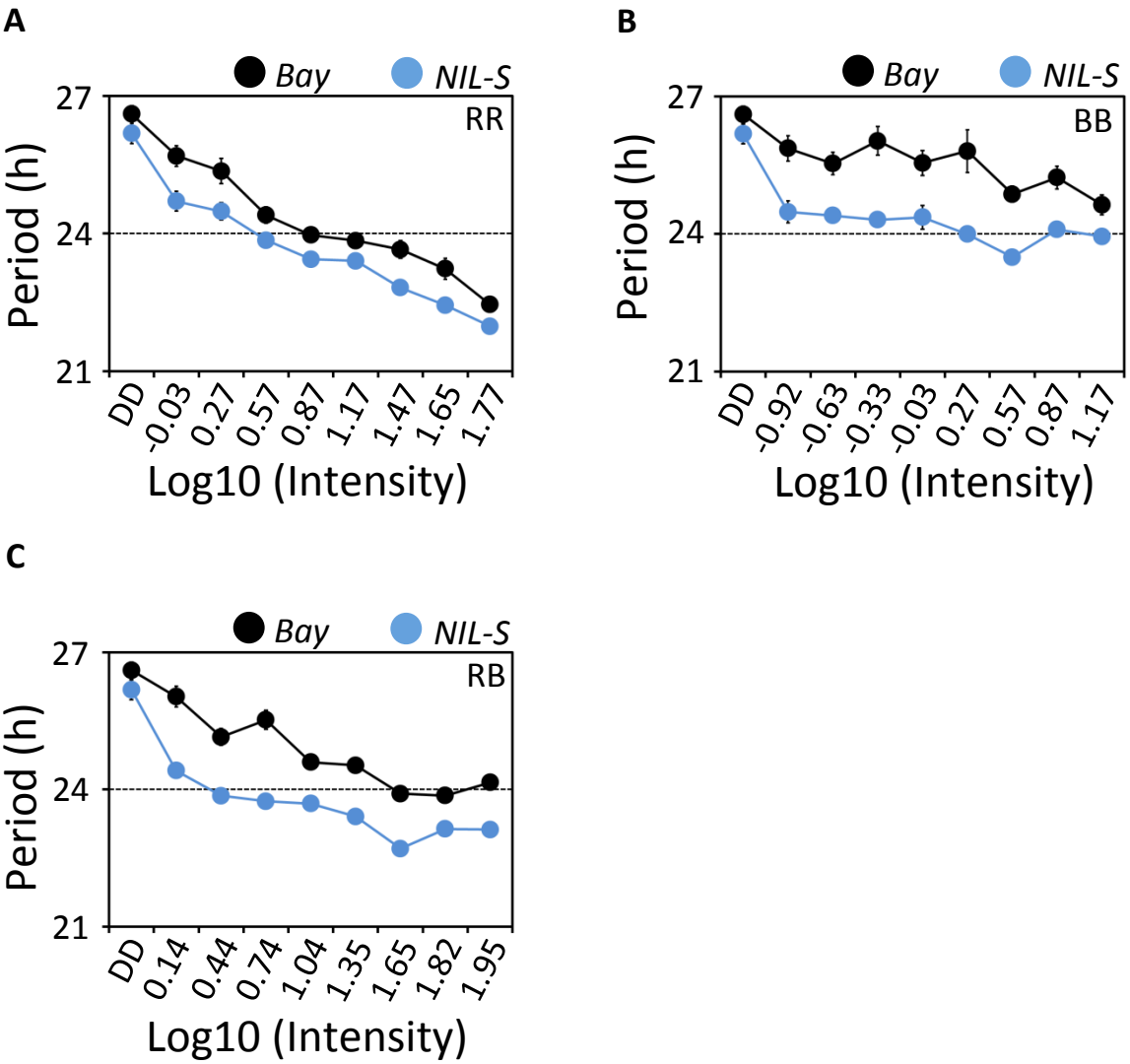
A
Bay
NIL-S
RR
27
24
21
Period (h)
DD
-0.03
0.27
0.57
0.87
1.17
1.47
1.65
1.77
Log10 (Intensity)
B
Bay
NIL-S
BB
27
24
21
Period (h)
DD
-0.92
-0.63
-0.33
-0.03
0.27
0.57
0.87
1.17
Log10 (Intensity)
C
Bay
NIL-S
RB
27
24
21
Period (h)
DD
0.14
0.44
0.74
1.04
1.35
1.65
1.82
1.95
Log10 (Intensity)

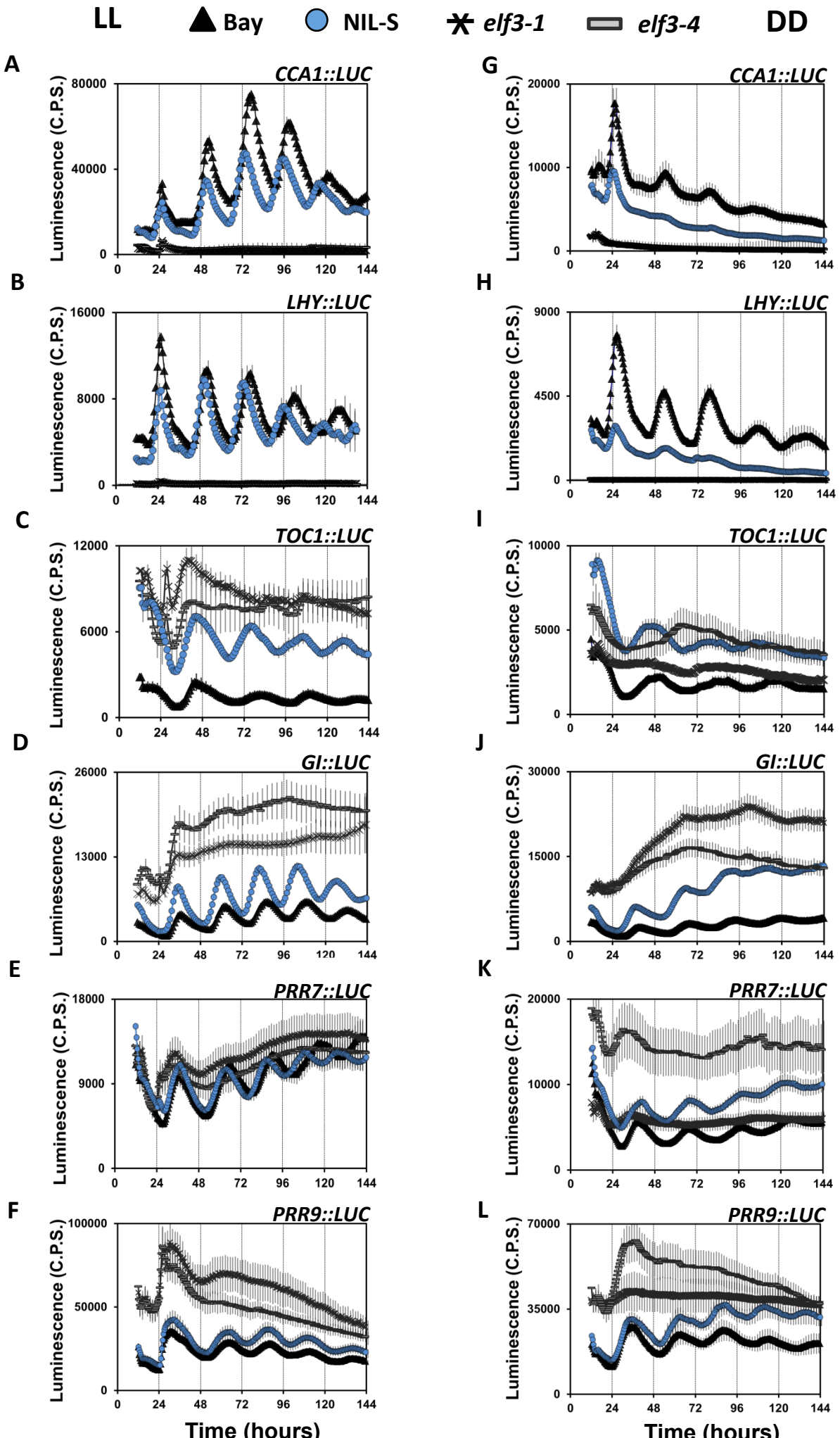
LL
Bay
NIL-S
elf3-1
elf3-4
DD
A
CCA1::LUC
B
LHY::LUC
C
TOC1::LUC
D
GI::LUC
E
PRR7::LUC
F
PRR9::LUC
G
CCA1::LUC
H
LHY::LUC
I
TOC1::LUC
J
GI::LUC
K
PRR7::LUC
L
PRR9::LUC
Luminescence (C.P.S.)
Time (hours)

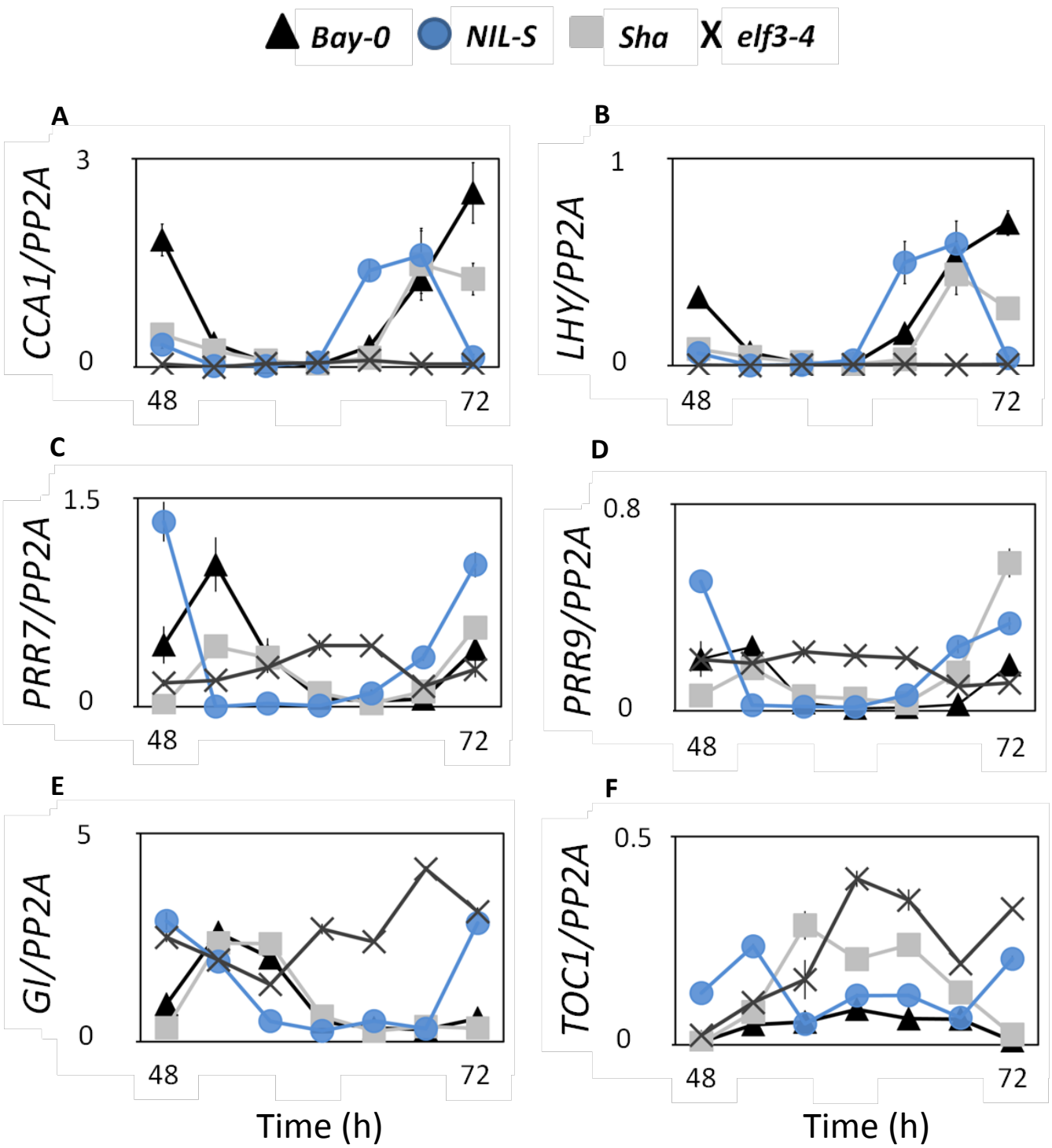
Bay-0
NIL-S
Sha
X
elf3-4
A
CCA1/PP2A
3
0
48
72
B
LHY/PP2A
1
0
48
72
C
PRR7/PP2A
1.5
0
48
72
D
PRR9/PP2A
0.8
0
48
72
E
GI/PP2A
5
0
48
72
F
TOC1/PP2A
0.5
0
48
72
Time (h)
Time (h)

A

ELF3 Bay-YFP

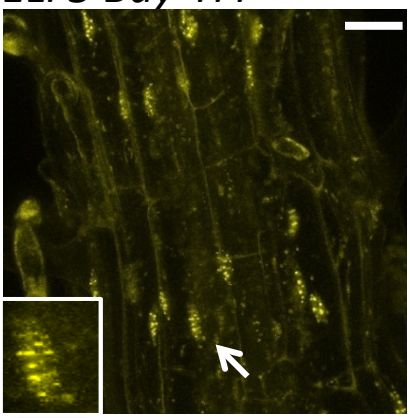

B

ELF3 Sha-YFP

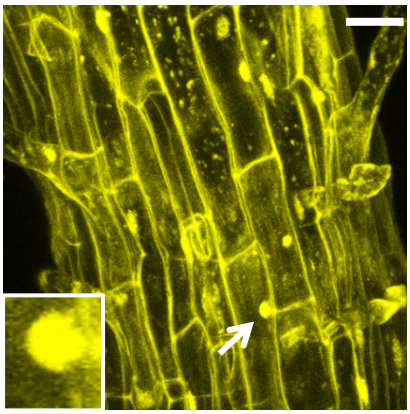

C

ELF3 Bay-YFP

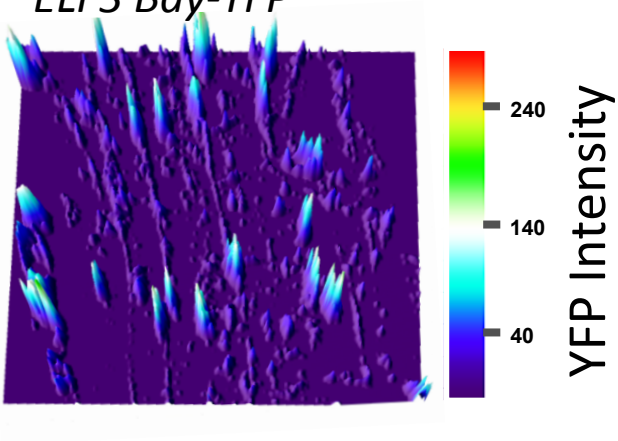

D

ELF3 Sha-YFP

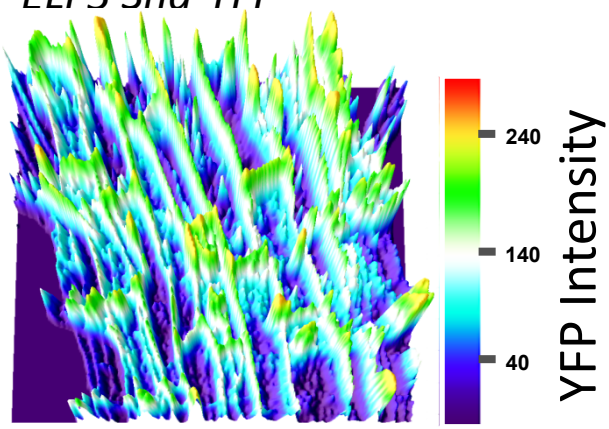

E

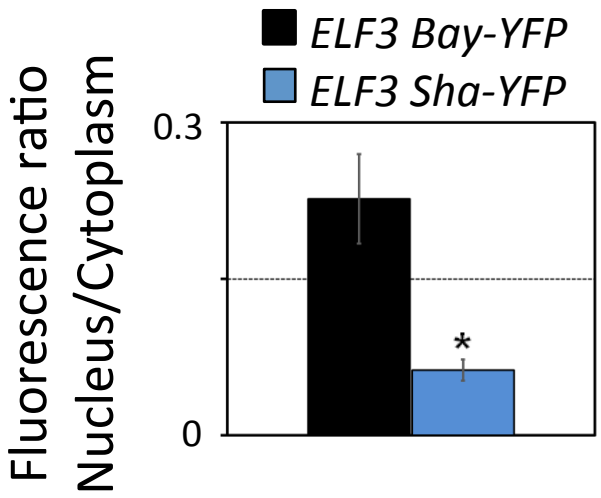

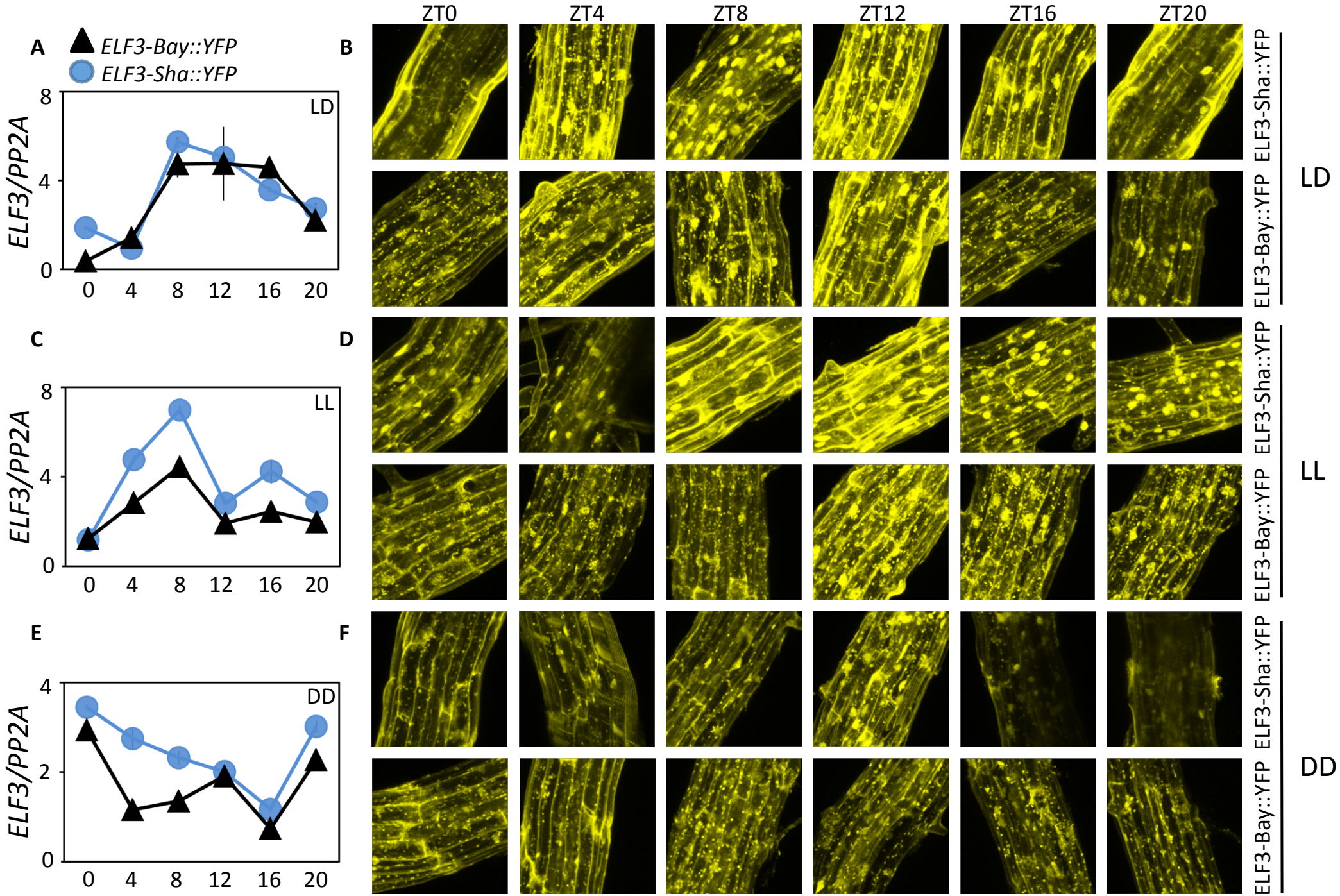
A
ELF3-Bay::YFP
ELF3-Sha::YFP
ELF3/PP2A
LD
0
4
8
12
16
20
B
ZT0
ZT4
ZT8
ZT12
ZT16
ZT20
ELF3-Sha::YFP
ELF3-Bay::YFP
LD
C
LL
D
E
DD
F

A

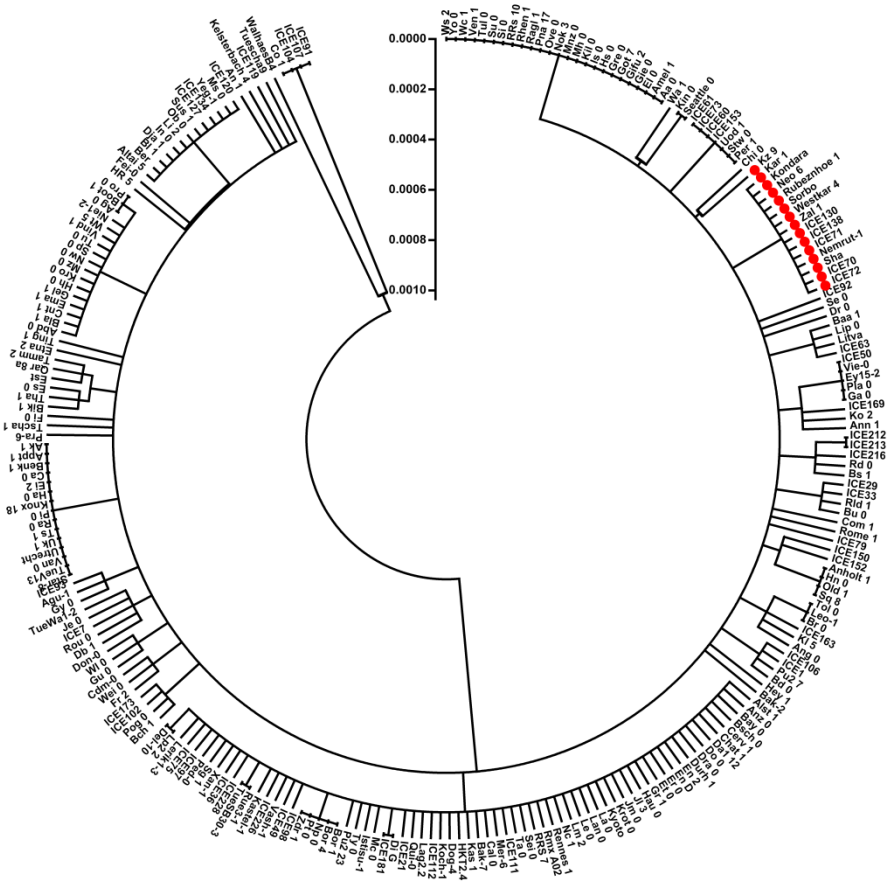
0.0000
0.0002
0.0004
0.0006
0.0008
0.0010

B

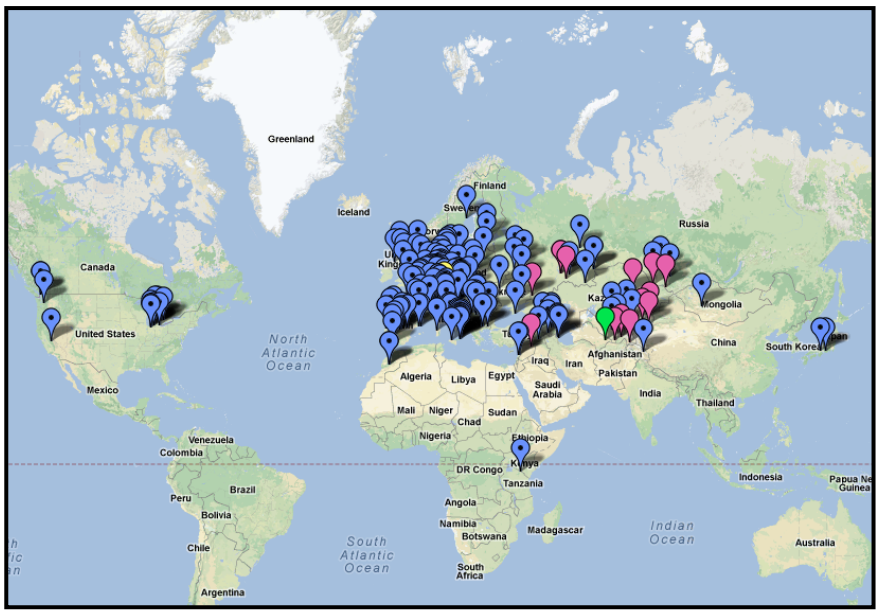
Greenland
Iceland
Finland
Russia
Canada
United States
Mexico
North Atlantic Ocean
Mongolia
China
South Korea
Afghanistan
Iran
Iraq
Pakistan
India
Thailand
Algeria
Libya
Egypt
Saudi Arabia
Mali
Niger
Chad
Sudan
Nigeria
Ethiopia
Kenya
DR Congo
Tanzania
Angola
Namibia
Botswana
Madagascar
South Africa
Venezuela
Colombia
Brazil
Peru
Bolivia
Chile
Argentina
South Atlantic Ocean
Indian Ocean
Indonesia
Australia